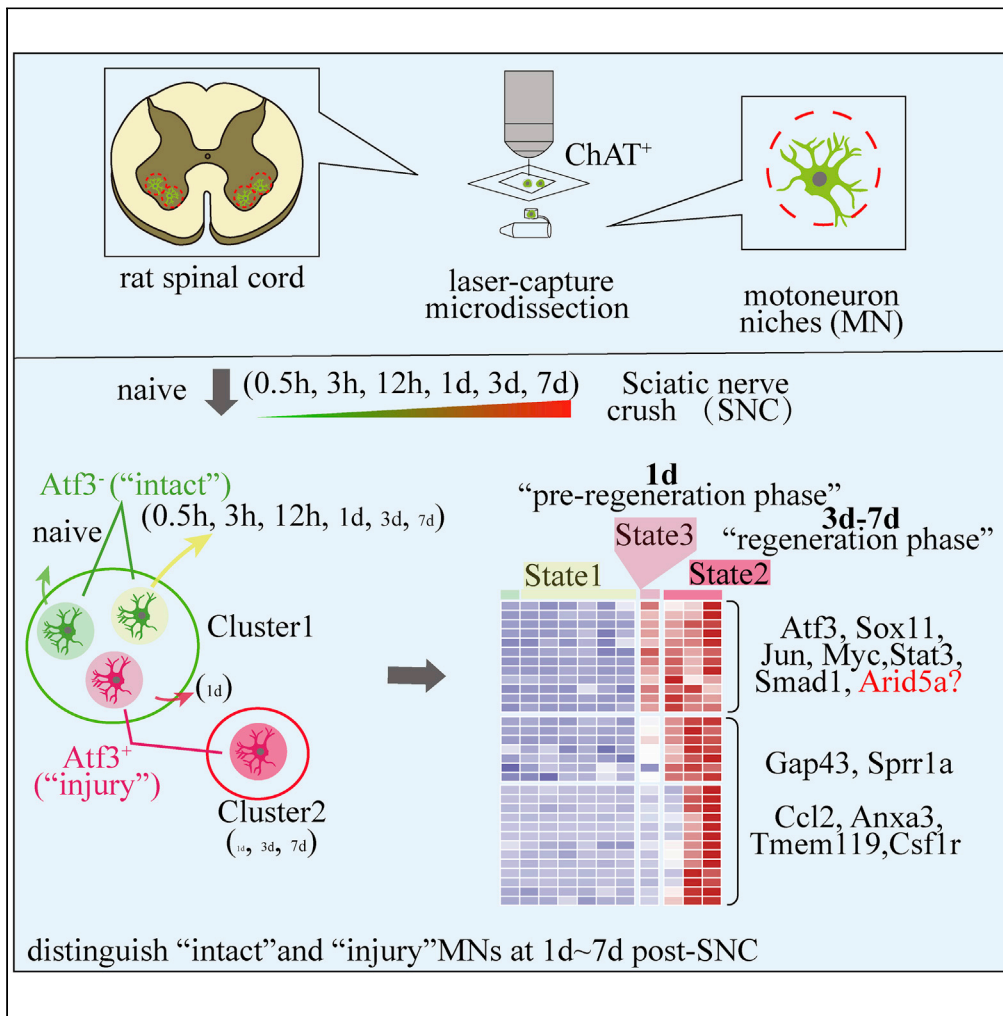


Article

Deciphering the dynamic niches and regeneration-associated transcriptional program of motoneurons following peripheral nerve injury



Yu Zhang, Lian Xu, Xiaodi Li, ..., Tao Zhang, Xiaosong Gu, Jian Yang

nervegu@ntu.edu.cn (X.G.)
dna2009@ntu.edu.cn (J.Y.)

Highlights

Transcriptional landscape of motoneurons (MNs) and its niches upon axonal injury

High dynamic niches and cell heterogeneity around injured and the regenerating MNs

Screen critical master regulators that may initiate regeneration program in MNs

Knockdown of Arid5a significantly reduces neurite outgrowth *in vitro*



Article

Deciphering the dynamic niches and regeneration-associated transcriptional program of motoneurons following peripheral nerve injury

Yu Zhang,^{1,3} Lian Xu,^{2,3} Xiaodi Li,¹ Zhifeng Chen,² Jing Chen,² Tao Zhang,¹ Xiaosong Gu,^{1,2,*} and Jian Yang^{2,4,*}

SUMMARY

Robust axon regeneration of motoneurons (MNs) occurs in rodent models upon peripheral nerve injury (PNI). However, genome-wide dynamic molecules and permissive microenvironment following insult in MNs remain largely unknown. Here, we firstly tackled by high-coverage and massive sequencing of laser-dissected individual ChAT⁺ cells to uncover molecules and pro-regenerative programs of MNs from injury to the regenerating phase after PNI. “Injured” populations at 1d~7d were well distinguished and three response phases were well defined by elucidating with several clues (*Gap43*, etc). We found remarkable changes of genes expressed by injured motoneurons to activate and enhance intrinsic axon regrowth or crosstalk with other cellular or non-cellular counterpart in the activated regenerative microenvironment, specifically microglia/macrophage. We also identified an injury and regeneration-associated module and critical regulators including core transcription factors (*Atf3*, *Arid5a*, *Klf6*, *Klf7*, *Jun*, *Stat3*, and *Myc*). This study provides a vital resource and critical molecules for studying neural repair of axotomized motoneurons.

INTRODUCTION

Peripheral nerve injury (PNI) is a common and severe clinical problem (Li et al., 2020b). Unlike limited regenerative capacity after CNS injury, axons of sensory and spinal motor neurons could regenerate and rebuild neuromuscular connections after PNI. Extensive studies have explored molecular changes and cellular heterogeneity in sensory neurons after PNI (Avraham et al., 2020; Renthall et al., 2020; Wang et al., 2021). However, limited studies have investigated those in spinal motoneurons (MNs) after PNI. Rodent sciatic nerve crush (SNC) injury is a well-characterized and robust model for studying peripheral nerve regeneration. In addition to the activation of the intrinsic regrowth program, the microenvironment also plays important roles in the successful axon regeneration, including resident glia, peripheral infiltrated immune cells (e.g. macrophage), vascular cells, and extracellular matrix homeostasis (Lei et al., 2012; Scheib and Hoke, 2013). A pioneering study has explored molecular change under translating in MNs using RiboTag; ChAT^{Cre} mouse model at 7 days post-SNC (Shadrach et al., 2021). However, this only covered limited mRNA forming their protein products and dynamic gene expression at the genome-wide level in MNs in the first seven days when undergoing dramatic change in gliosis and angiogenesis (Milich et al., 2021; Yu et al., 2019) after injury is still unknown.

Laser capture microscopy (LCM) combined with antibody rapid staining could capture cell types of interest *in situ* and coupled with Smart-seq2 (LCM-seq) could provide the accurate quantification of gene expression in dissected cells (Nichterwitz et al., 2016). LCM-seq has been successfully applied in studies of nervous system diseases, including Parkinson disease and amyotrophic lateral sclerosis (ALS) (Aguila et al., 2021; Nichterwitz et al., 2016, 2020). Unlike other cell isolation methods, such as fluorescence-activated cell sorting and microfluidics, LCM could harvest target cells from the microenvironment without dissociation of the tissue and preserved *in situ* spatial information (Nichterwitz et al., 2016). Though inevitable encompassing close its neighboring cells or non-cells around a target cell, LCM-seq just also provides additional information for its microecology.

MNs are large and sparse neurons in the ventral horn of the spinal cord which is difficult and inefficient to obtain sufficient and qualified MNs. Moreover, dynamic cellular heterogeneity around MNs during injury

¹School of Medicine and Holistic Integrative Medicine, Nanjing University of Chinese Medicine, Nanjing 210000, China

²Key Laboratory of Neuroregeneration of Jiangsu and Ministry of Education, Co-innovation Center of Neuroregeneration, NMPA Key Laboratory for Research and Evaluation of Tissue Engineering Technology Products, Nantong University, Nantong 226001, China

³These authors contributed equally

⁴Lead contact

*Correspondence: nervegu@ntu.edu.cn (X.G.), dna2009@ntu.edu.cn (J.Y.)
<https://doi.org/10.1016/j.isci.2022.104917>



and regeneration that nuclei isolation would lose substantial information. Thus, we employed LCM-seq to investigate the dynamic expression profile of spinal MNs soma and its minimum niches during axonal injury and regeneration. We investigated six timepoints post-SNC and the naive rat with approximately a single MN resolution (a motor neuron was contained in a sample). Comparison with another study (Shadrach et al., 2021) in gene expression of injured MNs and our immunostaining indicated the high quality of our data in reproducibility and accuracy. In the SNC rodent model, not all dorsal root ganglion (DRG) neurons or motoneurons are axotomized (~50%) (Holland et al., 2019; Shadrach et al., 2021). Based on clustering analysis and expression of neuronal injury marker (*Atf3*), we could well distinguish “intact” and “injured” MNs at 1, 3, and 7 days and estimated axotomized MNs ratio were approximated to previous studies (Holland et al., 2019; Shadrach et al., 2021). We found numerous robustly differentially expressed genes (DEGs) reported as regeneration-associated genes (RAGs) in DRG after PNI was robustly upregulated in “injured and regenerating” MNs by comparison with the naive and “intact” MNs. We also demonstrated highly dynamic microenvironments around “injured and regenerating” MNs with dramatic changes of genes related to the response of MNs, microglia/macrophage, vascular cells, and extracellular matrix reorganization. We also demonstrated critical regulators and a potential injury and regenerative-related co-expression module post-SNC. Specifically, we found a candidate master regulator (a transcription factor and RNA-binding protein, *ARID5A*) which may be associated with axon regeneration, presenting robust upregulation in injured neurons (including sensory and motor neurons) and co-expression with other well-known regulators (*Atf3*, *Klf6*, *Myc*, and *Sox11*) and significantly inhibiting neurites outgrowth of primary sensory neurons by knock-down of *Arid5a* *in vitro*. Finally, we present a web-based resource for easily exploring gene expression of MNs after PNI (MNNiches-seq). Our dataset not only provides the first temporal-spatial profile of individual MNs and its niche providing dynamic microenvironment information during axonal injury and regeneration, which are crucial for studying nerve regeneration and motoneuron degeneration disease, such as ALS.

RESULTS

Two distinct clusters were revealed by LCM-seq

We employed a sciatic nerve crush (SNC) rat model, and investigated timepoints: 0.5, 3, 12 h, 1 d, 3 d, and 7 d (hours/days), and compared to that from naive rats to study molecular dynamics for axonal injury and regeneration (Figure 1A). Motoneurons located in the ventral anterior horn of the lumbar spinal cord (L4/5) were labeled using rapid immunofluorescent staining of ChAT antibody and a circular region of the diameter around 1.5–2 times of a large motoneuron soma was cut using LCM under direct microscopic visualization, subjected to Smart-Seq2, and sequenced (Figures 1A and S1). Finally, a total of 700 samples were sequenced successfully with a depth of 44–134 million clean reads per sample. Samples with low expression of *Chat* (FPKM < 1) were discarded and left 682 samples (94–104 per condition) and a total of 16,163 protein-coding genes were expressed, at least three samples in one group (FPKM ≥ 1, 12,098–13,074 genes per condition, Figure 1C). Pearson’s correlation analysis showed a high correlation among dissected samples in each condition (Figure 1B). Neuronal activity was estimated with the AUCell package using neuronal markers (Aibar et al., 2017; Cahoy et al., 2008) and showed a high neuronal signature with an AUC score of 676 samples (~99%) greater than the estimation (0.12, Figure 1D). Besides, high expression of markers for alpha motoneurons (*Rbfox3* and *Spp1*) and low expression of the marker for gamma motoneurons (*Htr1a*) demonstrated that dissected samples here almost encompassed alpha motoneurons (Figure S2). Dimension reductions analyses demonstrated a clear two separated clusters with one consisting of naive samples and early injured samples (0.5–12 h) and most samples from 1 day (93.9%) and samples (47.9%–62.9%) from 3 to 7 days, while the other consisting of 37.1% and 52.1% of samples from 3 to 7 days, respectively (Figures 1E and 1F). Identification of the top 20 markers showed that genes with high expression in cluster 2 were related with the response of neuron and glia to axonal injury, such as neuronal released factors (*Atf3*, *Ccl2* (Shadrach et al., 2021), *Reg3b* (Namikawa et al., 2005), and *Serpina3n* (LOC299282) (Vicuna et al., 2015)) microglial activation (*Reg3b* (Li et al., 2020a; Namikawa et al., 2005), *C1qa*, *Csf1r*, *Anxa3* (Zhang et al., 2021), and *Lyz2*), and astroglial activation (*Gfap*, *Il33* (Gadani et al., 2015b), and *Timp1* (Ogier et al., 2005)). *Anxa3* (annexin A3) was most expressed in microglia/macrophages and endothelial cells in the spinal cord (Blum et al., 2021) and functions in inflammation, angiogenesis, and rat liver regeneration (Hara-shima et al., 2008; Park et al., 2005). Immunostaining of ANXA3 showed obviously increased ANXA3⁺ cells in ventral horn were detected as early as 1 day, but close contact between ANXA3⁺ cells and motoneurons were obviously increased at 3 and 7 days reflected by adhesion to the neuronal perikaryon, which is consistent with the result of IBA1 immunostaining (Figures 1I and S3), suggesting increased crosstalk in neuron-microglia. This was generally consistent with our sequenced data. The top 20 upregulated genes in cluster 2 also included known RAGs (*Atf3*, *Gap43*, *Ngfr*, *Timp1*, and *Ccl2*), energy metabolism (*Ldha*), ECM (*Timp1*)

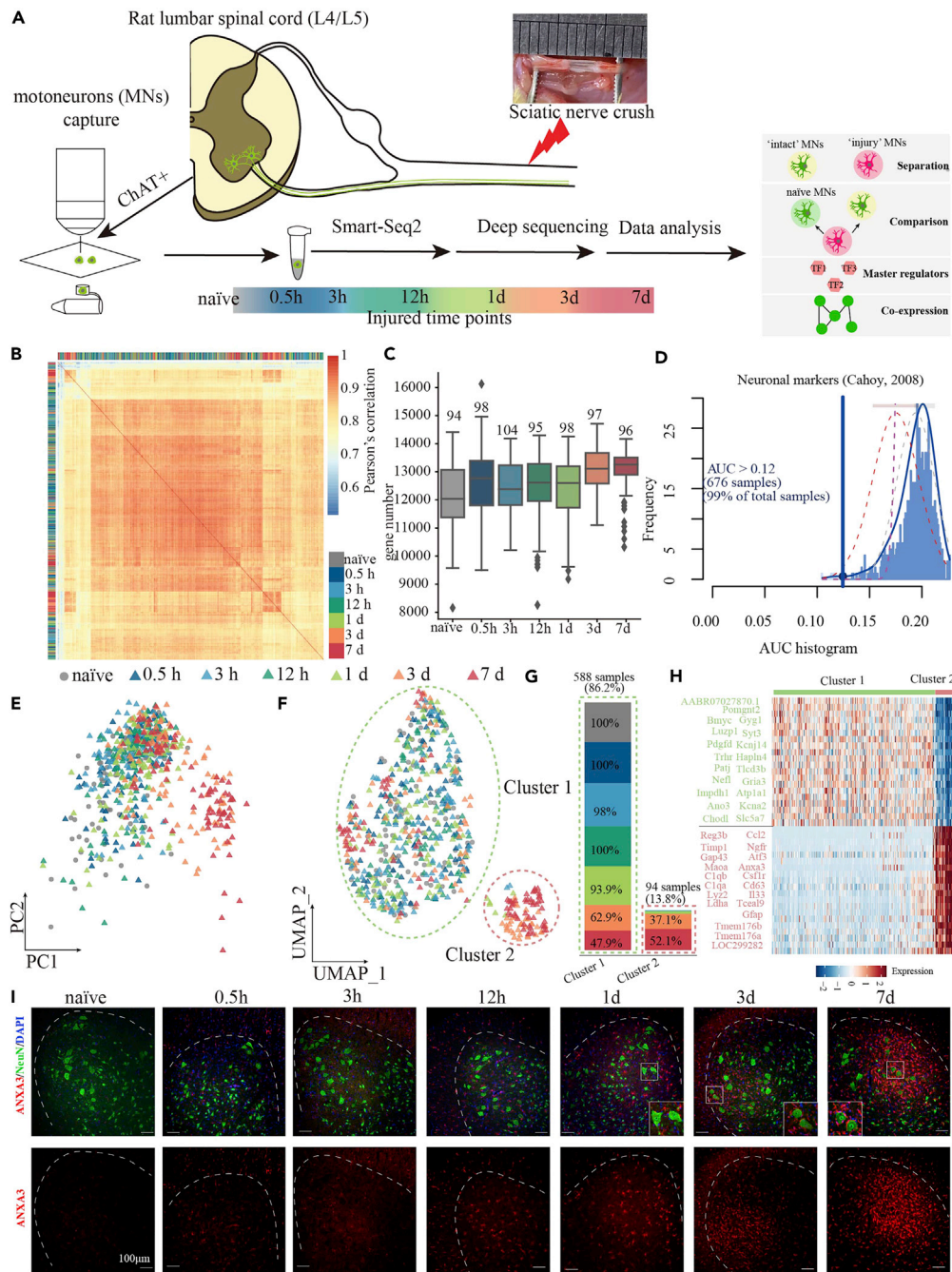


Figure 1. Two distinct clusters in ventral lumbar spinal motoneurons post-SNC

(A) Overview of the investigated timepoints and workflow of the experiment.
 (B) Pearson's correlations among samples captured based on expressed genes (gene with average FPKM >1 was kept).
 (C) Gene number identified per condition. The number above the boxplot represented the sample number.
 (D) Histogram of AUC score of neuronal markers reflecting the high activity of neuronal characteristics.
 (E) Principal component analysis (PCA) visualization of samples distribution.
 (F) UMAP clustering of samples. Two distinct clusters were shown.
 (G) The sample proportion of each group from different injury timepoints in two clusters.
 (H) Expression profiles of top 20 differential expression genes in either cluster 1 or cluster 2.
 (I) Immunostaining of ANXA3 (red) in rat ventral lumbar spinal cord at different injured timepoints post-SNC. Neuron and nuclear were labeled with NeuN (green) and DAPI (blue). Scale bar: 100 μm.

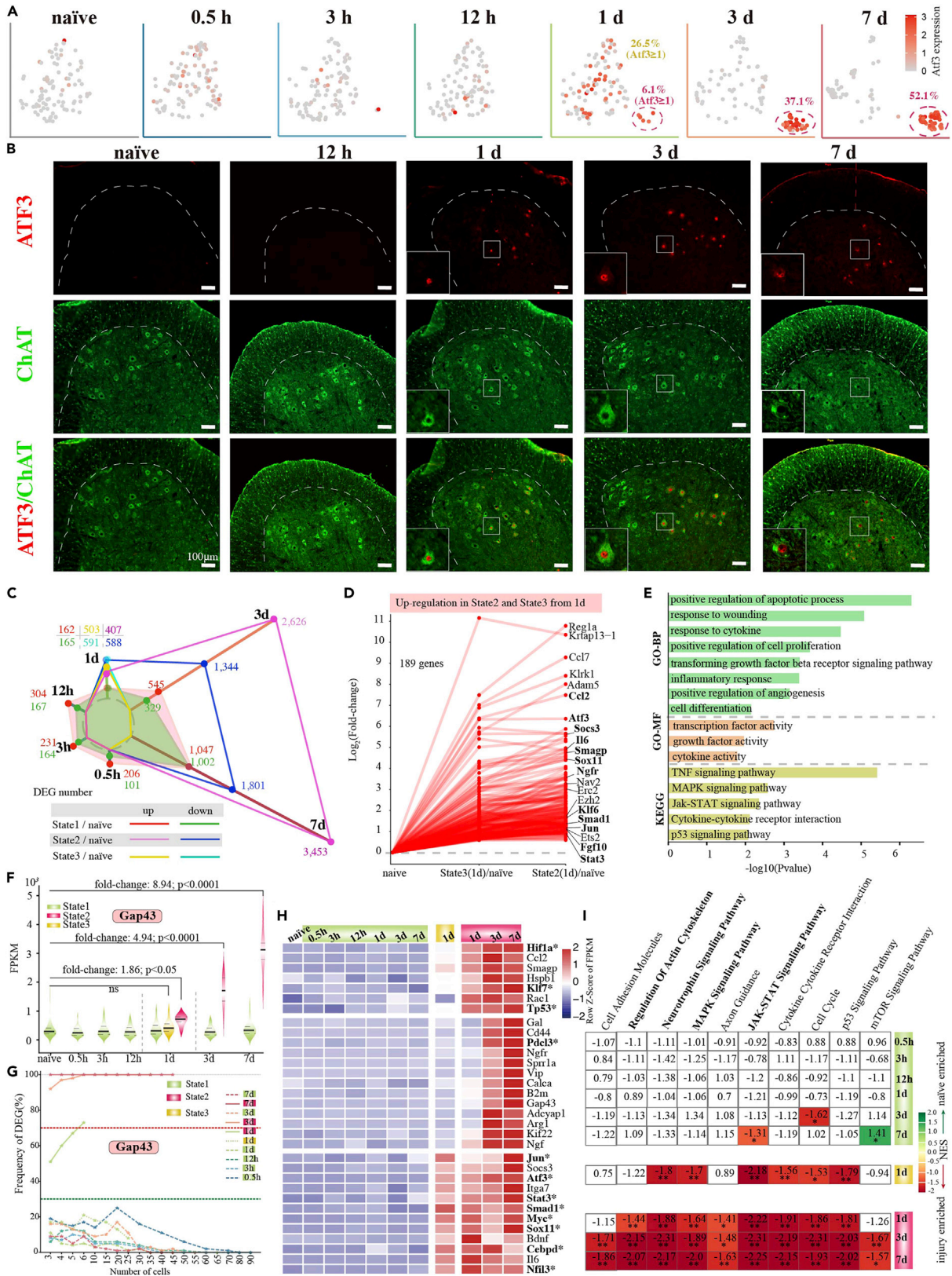


Figure 2. Three response stages in axonal injury and regeneration post-SNC

- (A) Separate UMAP plots of *Atf3* expression in samples collected from different post-injury timepoints. The ratio of *Atf3* expression ≥ 1 of cluster 1 and 2 at 1 day or ratio of cluster 2 at 3 and 7 days post-SNC was shown.
- (B) Immunostaining of ATF3 in the lumbar spinal cord from different post-injury timepoints.
- (C) The radar map depicts the gene number of DEGs ($P\text{-value} \leq 0.05$ and $|\log_2^{\text{fold-change}}| \geq \log_2^{1.5}$) at different injured time points in different states compared to the naive.
- (D) Significantly and consistently upregulated genes at 1 day post-SNC in samples from state 2 and state 3. DEGs with top rank or critical were labeled.
- (E) Functional enrichment analysis of consistently upregulated DEGs in 1 day post-SNC at state 2 and state 3.
- (F) *Gap43* expression at different states in different injured time points post-SNC.
- (G) Frequency of detected differentially expressed *Gap43* with 100 bootstrap DESeq2 with varied sample sizes.
- (H) Expression of well-established regeneration-associated genes collected from the literature. * indicated transcription factors.
- (I) Geneset enrichment analysis of well-known pathways related to regeneration. Terms with false discovery rates (FDR, $FDR < 0.25$) were highlighted with * (NOM $p < 0.05$) and ** (NOM $p < 0.01$).

and *Timp1* receptor (*Cd63*, a tetraspanin), and pro/anti-inflammation (*Reg3b*, *Ccl2*; *Il33*). *Timp1* interacting with *Cd63*-activating $\beta 1$ integrin signaling could activate cellular signaling cascades, promoting cell survival and migration and regulating cytoskeletal reorganization (Lee et al., 2014). Taken together, we suspected that samples in cluster 2 contained injured MNs and underwent regenerating as discussed below.

Three response stages were revealed by LCM-seq

Atf3 is a sensitive and specific neuronal marker with injured peripheral axons (Tsujino et al., 2000). Separate UMAP plots of *Atf3* expression showed high expression in samples from cluster 2 and also showed high expression in part samples from cluster 1 at 1 day post-SNC (Figure 2A). We found the expression of *Atf3* was greater than 1 in almost samples from cluster 2 while less than 1 in other samples except for part samples from cluster 1 at 1 day (26 samples, 26.5%, Figure 2A). Interestingly, this ratio (26.5%) was approximate to the estimation (~23.8%) of injured sensory neurons at 1 day post sciatic nerve injury (Rental et al., 2020). Only 1–2 samples in cluster 2 from 3 to 7 days showed expression of *Atf3* was less than 1 that we directly assigned based on the clustering results (Figure S4). Namely, 37.1% and 52.1% of “injured” MNs were estimated at 3 and 7 days respectively, which were also consistent with the estimation in motoneurons using ATF3-CreERT2 knockin mouse post-SNC ($45 \pm 2\%$ for 4 days) (Holland et al., 2019). Thus, we divided these samples into three response stages and termed these stages with stages 1–3 (namely 0.5–12 h, 1 day, and 3~7 days) and three states (states 1–3). *Atf3* was significantly upregulated with remarkable fold-change in state 2 and state 3 (81- to 82-fold at 1 day, 122-fold at 3 days, and 131-fold at 7 days) while no significance in state 1 (Figure S5). Our estimation is approximate to the fold-change (134-fold) of Rpl22^{HA} immunoprecipitation (IP) in ipsilateral motoneurons compared to the contralateral ones from RiboTag; ChAT^{Cre} mouse model at 7 days post-SNC (Shadrach et al., 2021), suggesting high reproducibility and accuracy of our data. Besides, we employed bootstrapping strategy to identify robust differential expression genes (DEGs) (Aguila et al., 2021) and showed remarkably robust ($\geq 90\%$) differential expression of *Atf3* in state 2 and state 3 (Figure S5). The SCENIC (Aibar et al., 2017) analysis showed that the activity of *Atf3* regulon was also significantly higher in state 2 and state 3, indicating *Atf3* was mostly activated as early as 1 day (Student's t test, $*p < 0.05$, $**p < 0.0001$, Figure S5). Immunolabeling of ATF3 in rat spinal cord upon axonal injury supported our sequencing results that ATF3 was expressed as early as 1 day and co-localized with the nucleus of part motoneurons, indicating injured MNs (Figure 2B). ATF3-positive injured MNs most located in ventral posterolateral nucleus were motor pools for innervation muscles of a limb.

Next, we analyzed DEGs by comparison with the naive to assess whether separation based on a single marker could well obtain a distinct expression profile that reflects cell states. The result showed a significant increase in DEG number after separation with approximately 2-fold of DEG numbers without separation (Figure S6). A smaller number of DEGs were detected in in state 1 from timepoints (0.5 h~1 day, <500 DEGs) than that detected from 3 (874 DEGs) and 7 days (2,049 DEGs) (Figure 2C). A larger DEG number was detected in state 2 and/or state 3 than that detected in the corresponding state 1. A similar DEG number in state 2 and state 3 was detected at 1 day, while a larger DEG number was detected in state 2 at 3 and 7 days, suggesting distinct expression profiles between 1 and 3 days/7 days. 189 and 104 genes showed consistent upregulation and downregulation in state 2 and state 3 at 1 day, respectively (Figure 2D), and upregulated genes were significantly enriched in terms of “response to wounding”, “cell proliferation”, “angiogenesis”, and several signal pathways, such as MAPK and Jak-STAT signaling pathways (Figure 2E). These evidences suggested that our sample separation could well represent distinct cell states by supporting with distinct expression profiles.

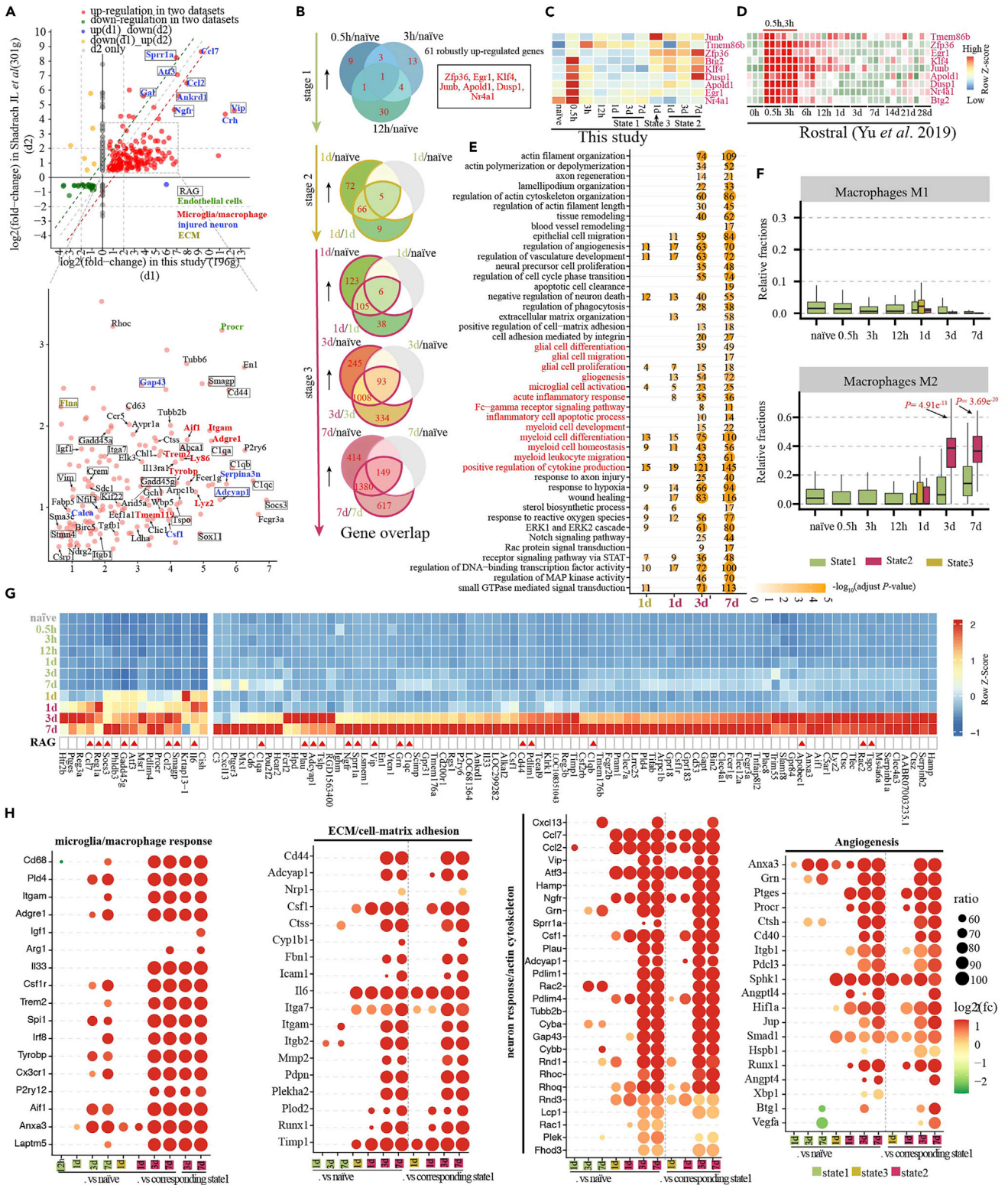


Figure 3. Robust DE-Gs in response to axon injury and regeneration

(A) Significant correlation of fold-change of DEGs between the study and our data at 7 days post-SNC.

(B) Venn diagram depicts the overlapped gene numbers by comparison with the naive or corresponding state 1 following SNC.

(C) Nine robust upregulated DEGs in our study.

Figure 3. Continued

(D) Expression of nine robustly upregulated DEGs in spinal cord injury dataset.

(E) GO enrichment of upregulated genes at 1, 3, and 7 days compared to the naive or corresponding state 1. DEG number annotated a term was shown within the dot.

(F) The relative fraction of macrophage subtypes estimated in our collected samples based on the CIBERSORT method.

(G) Top-ranked 100 robustly upregulated DEGs by considering both expression level and fold-change.

(H) Expression profiles of key genes related to important processes during axon injury and regeneration.

Gap43 is a proven marker labeling for developing and regenerating neurons. Our analysis of *Gap43* expression showed significant upregulation only in state 2 (1.86-fold at 1 day, 4.94-fold at 3 days, and 8.94-fold at 7 days, [Figure 2F](#)). The upregulated fold-change of *Gap43* is consistent with the estimation in MNs (1.96-fold at 1 day, 5.82-fold at 3 days, and 9.93-fold at 7 days) ([Shadrach et al., 2021](#)), confirming our data accuracy and suggesting the regenerating axon in samples from the cluster 2 population. *Gap43* was robustly upregulated in state 2 neither state 1 nor state 3 (frequency $\geq 50\%$, [Figure 2G](#)). Numerous RAGs (*Atf3*, *Gap43*, *Sprr1a*, *Jun*, *Sox11*, etc) with literature evidence showed significant upregulation in state 2 at 3 and 7 days, and some in state 2 and/or state 3 at 1 day ([Figure 2H](#)). Notably, important pro-growth transcription factors (*Atf3*, *Sox11*, *Stat3*, *Smad1*, *Jun*, and *Myc*) showed significant upregulation as early as 1 day in state 3 and maintain upregulation in state 2, while terminal RAGs, such as *Gap43*, *Hspb1*, *Sprr1a*, and *Ccl2*, showed only significant upregulation in state 2. This result indicated that state 3 from 1 day was the pre-regeneration phase that activated pro-regenerative TFs for the initiation of the regenerative program. Furthermore, most RAGs showed high expression in state 2 from 1 to 3 days, while part RAGs showed high expression in state 2 from 1 day, suggesting a gradual initiation of regenerating program and 1 day was a key point for successful regeneration.

In addition, we also investigated the enrichment of several important pathways related to regeneration, such as "Neurotrophic signaling pathway", "MAPK signaling pathway", "JAK-STAT signaling pathway", and reflecting axon regeneration "Regulation of actin cytoskeleton". The result showed pro-regenerative pathways were significantly enriched in state 2 and state 3, but not in state 1 compared to the naive ([Figure 2I](#)). Actin cytoskeleton-related term was significantly enriched in state 2. This result suggested that state 3 from 1 day is a pre-regeneration phase while state 2 was regenerating phase.

Collectively, dissected samples could be divided into two clusters and three response phases which could be categorized as "early stress response phase" (stage 1, 0.5–12 h), "pre-regeneration phase" (1 day), and "regeneration phase" (3~7 days) in our investigated injured timepoints.

Robustly differentially expressed genes of MN niches in response to axonal injury

We next performed differential expression analysis by comparison with the naive. We compared our results (state 2 from 7 days) with DEGs (301 out of 342 with ortholog in rat were considered) identified by comparing expression of Rpl22^{HA} IP in injured and regenerating MNs with the uninjured in mouse spinal cord at 7 days post-SNC ([Shadrach et al., 2021](#)). Significant correlation between these two datasets (Pearson's correlation: 0.58, p-value < 2.2e-16) was observed based on the fold-change of common DEGs compared to the corresponding control. 189 out of 196 (96.2%) overlapped DEGs showed consistent either upregulation or downregulation, including *Atf3*, *Bst2*, and *Cyp1b1* ([Figure 3A](#) and [Table S1](#)). Of the common DEGs, we found dramatical upregulation of genes was released or expressed by injured neurons, such as *Atf3*, *Ccl7*, *Ccl2*, *Ngfr*, *Vip*, *Crh*, *Gal*, *Sprr1a*, *Ankrd1*, *Csf1*, *Adcyap1*, and *Serpina3n*. Besides, we also found genes related to other cellular (endothelial cells, microglia/macrophage) or non-cellular (ECM) were present, suggesting their important roles in axon regeneration. Our result showed a small number of DEGs (<500) at early injury (0.5–12 h) and state 1 from 1 day ([Figure 2C](#)) under the relaxing threshold. Though a relatively large number of DEGs (847–2,049) were detected in state 1 at 3 and 7 days ([Figure 2C](#)). However, GO enrichment showed that DEGs in state 1 at 3 and 7 days were almost enriched in terms related to inflammation and immune response, such as "positive regulation of cytokine production" and "regulation of inflammatory response" ([Figure S7](#) and [Table S2](#)). Axonal injury triggers sterile inflammation with peripheral immune cell infiltration, migration, proliferation and differentiation, and CNS microglia activation, proliferation ([Gadani et al., 2015a](#)), forming an inflammatory milieu. Thus, DEGs detected in state 1 from 3 to 7 days may be explained by the physiological response to detrimental stimuli in "intact" motoneurons. Moreover, captured and discriminated "intact" motoneurons and its minimal niches at 1, 3, and 7 days provide a valuable control for further screening crucial molecules involved in axon regeneration.

We next employed bootstrap strategy (Aguila et al., 2021) to identify robust and reliable DEGs (average frequency $\geq 50\%$). 80 robust DEGs presented in early injury (61 up- and 19 downregulated genes, 0.5–12 h, Figure 3B and Table S3). We found genes, *Zfp36*, *Egr1*, *Klf4*, *Junb*, *Apold1*, *Dusp1*, and *Nr4a1*, were also significantly upregulated at early injury response in spinal cord injury (Yu et al., 2019) (0.5~3 h, Figures 3C, 3D, and S8). Most of these seven genes were expressed in endothelial and pericyte cells (Milich et al., 2021) (Figure S9), including genes related with angiogenesis (*Apold1*, endothelial cell-specific) and reported as early stress response (*Egr1* and *Nr4a1* (Shaked et al., 2015)) and related with inflammation (*Zfp36*, *Dusp1*, *Nr4a1*, *Junb*, *Klf4*, and *Egr1*) (Shaked et al., 2015; Trizzino et al., 2021), suggesting the immediate response of vascular network and inflammation around motoneurons after injury.

Robust DEGs at 1, 3, and 7 days were further screened with either up- or downregulation in comparison with the naive or corresponding state 1 group (upregulation was shown in Figure 3B). A total of 4,916 robustly up- or downregulated genes were identified (Table S4). GO enrichment of upregulated genes (Figure 3E and Table S5) showed that terms related to inflammation and immune response were the most enriched at 3 and 7 days, such as “positive regulation of cytokine production” and “acute inflammatory response”. We also found terms related to myeloid cells (differentiation, migration, and homeostasis) were significantly enriched (Figure 3E). To estimate the abundance of immune cells around a motor neuron upon injury, we employed the CIBERSORT (Newman et al., 2015) deconvolution analysis, a tool estimated the abundances of member cell types in a mixed cell population. The result showed a significantly increased cell fraction of M2 macrophage at 3 and 7 days, specifically in state 2, based on a leukocyte gene signature matrix (LM22), suggesting accumulation of anti-inflammation macrophage around injured and regenerating motoneurons (Figures 3F and S10). We found microglia/macrophage markers showed robust upregulation at 1, 3, and 7 days, specifically at 3 and 7 days, such as *Tmem119*, *P2ry12*, *Aif1* (IBA1), *Csf1r*, *Cx3cr1* (Figure 3G) and several (*Tmem119*, *Trem2*, *Aif1*, *Itgam* (Cd11b), *Adgre1* (F4/80), *P2ry6*, and *Tyrobp* (DAP12)), were also present in another study (Shadrach et al., 2021) (Figure 3A). Significant robust upregulation expression of microglia related in comparison with the naive and “intact”, suggesting the importance of microglia-motoneuron crosstalk in axonal injury and repair, such as genes involved in activation (*Csf1*, *Spi1*, *Irf8*, *Laptm5*, *Reg3b*, etc), migration (*Trem2*, *Csf1*, and *P2ry12*), proliferation (*Il33*), and transition from M1 to M2 (*Arg1* and *Igf1*, Figure 3H).

We also found terms related to axon regrowth were the most enriched in “injured and regenerating” at 3 and 7 days, such as actin cytoskeleton organization (*Pdlim1*, 4, and *Rnd1*) and microtubule polymerization (*Tubb2b*, Figures 3F and 3H). We found 23 RAGs with literature evidence present at the top 100 of ranked upregulated genes, including injured MNs released peptide/hormone (*Vip*, *Adcyap1*), cytokine (*Ccl2*, *Ccl7*, and *Tslp*), growth factors/receptor (*Ngfr* and *Grn*), and regenerating axon (*Sprr1a*, Figure 3G). Of which, injury-induced cytokines, *Ccl2* (322-fold at 3 days and 243-fold at 7 days) and *Ccl7* (788-fold at 3 days and 624-fold at 7 days), proven mostly released by injured neurons to activate or recruit microglia/macrophage for enhancing axon regeneration were presented at the top 10 ranked upregulation, which was consistent with the study (Kwon et al., 2015; Shadrach et al., 2021). *Vip* (immunoreactive vasoactive intestinal peptide) and *Adcyap1* (also known as PACAP), released by neurons, could promote and accelerate early myelination and axon regrowth after PNS injury (Woodley et al., 2019; Zhang et al., 2002). We found low expression of *Vip* and *Adcyap1* in the naive, early injury (0.5 h~1 day), and “intact” neurons at 3 and 7 days (<1 FPKM) but dramatic increased at state 2 from 3 to 7 days (17–39 FPKM). *Adcyap1* exerts pleiotropic roles with neurotrophic factor, neuromodulator, and neurotransmitter and could enhance neurite growth by binding its predominant receptor, *Adcyap1r1* (PAC1), in human sensory neurons (Baskozos et al., 2020).

Except for the response from glia and neurons, we also found genes related to angiogenesis, such as *Procr*, *Hif1a*, *Cd40*, *Grn*, and *Angptl4* (Figure 4H). *Procr* (Endothelial protein C receptor precursor), a marker of endothelial stem cells, was only significantly upregulated at state 2 (20-fold at 1 day, 42- to 47-fold at 3 and 7 days), and upregulation was also observed in the study (9-fold at 7 days, Figure 3A) (Shadrach et al., 2021). Neurovascular units are critical to nerve regeneration and angiogenesis plays vital roles in wound healing by neurotrophic support, such as released growth factors (*Vegfa* and *Vegfb*) contributing a permissive microenvironment for axonal regrowth (Guaiquil et al., 2014). Injury induces hypoxia condition that activation of *Hif1a* (hypoxia-inducible factor, 3.6- to 3.7-fold at 3 and 7 days), a critical regulator in regenerating neurons, orchestrate various angiogenic factors, such as VEGF, bFGF, angiopoietins, and angiopoietin-like (ANGPTL) proteins to enhance nerve regeneration (Cho et al., 2015; Inoue et al., 2014).

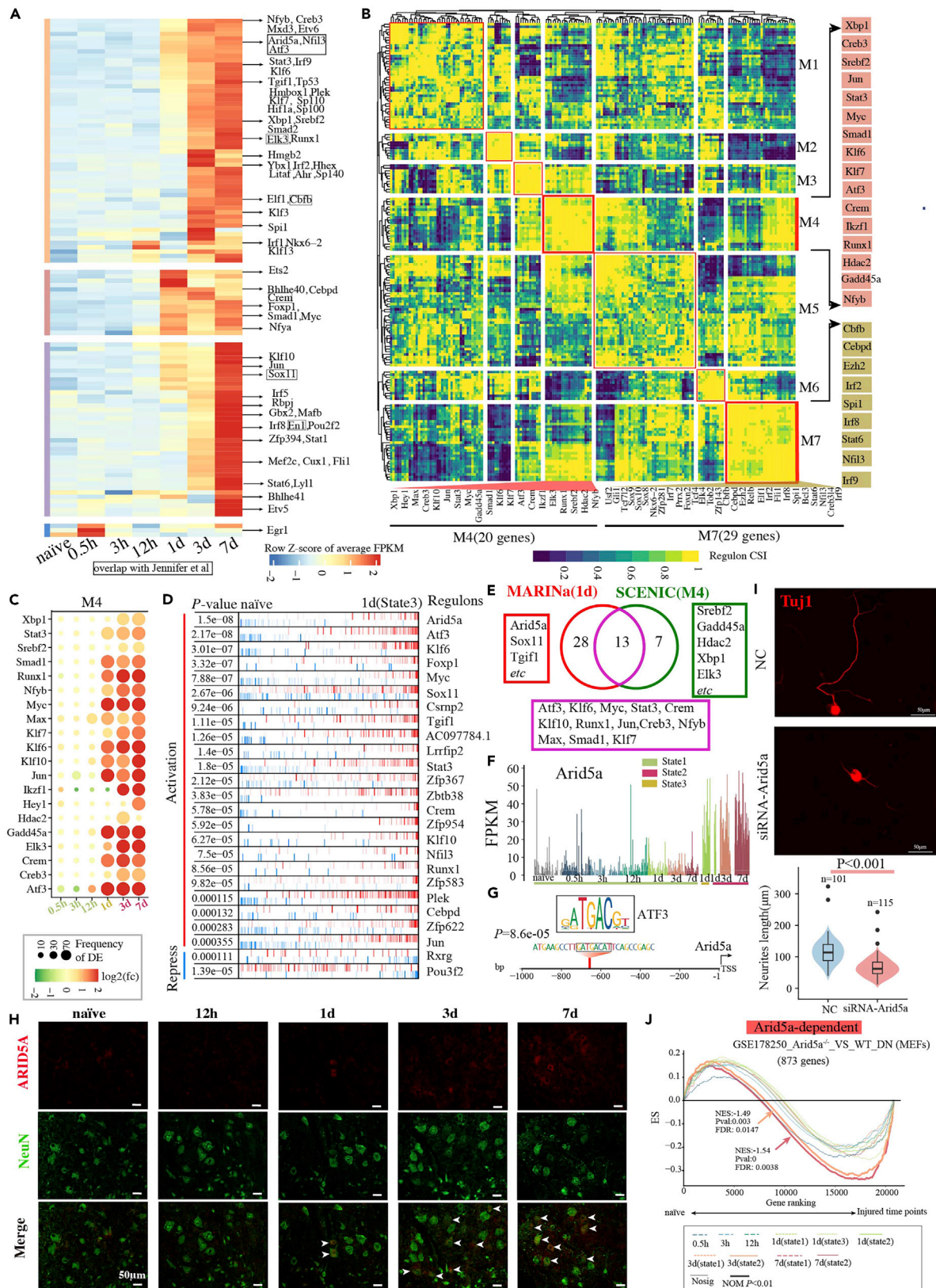


Figure 4. Vital TFs and core regulons in axonal injury and regeneration

- (A) Three of five clusters of TF expression patterns.
- (B) Heatmap plot depicts clustering among regulons inferred from SCENIC based on connection specificity index (CSI) based on AUC score of regulons.
- (C) Frequency and log₂-transformed fold-change of key regulators in M4 from Figure 4A across different injured time points compared to the naive. Regulators of regulons from M4 were shown at the bottom of the heatmap and key regulators were shown at the right of the heatmap. Only samples of state 3 from 1 day and state 2 from 3 to 7 days were considered.
- (D) The top 25 regulons at 1 day were identified by the master regulator analysis algorithm (MARINA) compared to the naive. Vertical bars indicated positions of the targets belonging to each TF's regulon and colors indicated the Spearman's correlation between the expression profiles of the TF and its targets (blue: negative correlation; red: positive correlation).
- (E) Venn diagrams depict the overlap of candidate master regulators inferred from MARINA and SCENIC. Regulators with FDR <0.05 inferred by MARINA at 1 day were selected. Co-operated regulators at M4 inferred by SCENIC were selected.
- (F) Expression of *Arid5a* at different injured time points at distinct states. Each line depicts a sample.
- (G) Binding sites between ATF3 and *Arid5a* were identified by the FIMO program. Red blocks indicated ATF3-binding sites. Numbers on the x axis represent the base number 5' upstream from *Arid5a* transcription start sites.
- (H) Immunostaining of ARID5A in the ventral horn of the rat lumbar spinal cord at different timepoints post-injury.
- (I) Knockdown of *Arid5a* by siRNA significantly reduced the total neurite length in primary DRG neurons. Up: representative images of *Arid5a* knockdown (siRNA-*Arid5a*) and negative control (NC) in culture neurons. Down: total neurite length per DRG neuron after *Arid5a* knockdown was quantified. The significant difference was performed using Student's t-test.
- (J) Enrichment score distribution of geneset (873 ortholog genes in rat with significantly downregulated in *Arid5a* knockout mice independent of IL6 stimulation) at different injured time points at distinct states against the naive. Line colors depict injured time points and shapes depict distinct states. Line width depicts enrichment with significant (thick) or not (thin).

Thus, robust upregulation of proangiogenic genes in endothelial cells may provide a permissive microenvironment to promote axon regeneration.

We also found terms related to ECM, such as cell-matrix adhesion and cell adhesion mediated by integrin, were significantly enriched at 3 and 7 days (Figure 3E). ECM is composed of fibrous proteins (e.g. collagen and glycosaminoglycans) and other proteins secreted by neighboring cells or exocytosis, which is important for guiding regenerating axons, regulating cell behavior, and enhancing cell-cell interaction (Roumazeilles et al., 2018; Yu et al., 2008). Cell adhesion molecules, such as interacting between immune cells-matrix (*Itgam* and *Itgb2*), neuron-matrix (*Csf1* and *Adcyap1*), and endothelial-matrix (*Nrp1*) showed robust upregulation following SNC at 3 and/or 7 days.

Dynamic TFs and inference of co-operated key TFs related to axon regrowth

A total of 345 differentially expressed TFs (47.4% of 727 TFs with average FPKM ≥ 1) were identified by comparison with the naive. Of which, 176 TFs showed robust differentially expressed after axonal injury (frequency $\geq 50\%$, Figure 4A and Table S6) and were clustered into five distinct clusters. Three clusters (k1~3 in Figure 4A) showed significant upregulation in the "pre-regeneration phase" and/or "regeneration phase". We also found nine TFs (*Arid5a*, *Nfil3*, *Atf3*, *Crem*, *Sox11*, etc, Figure 4A and Table S1) present in DEGs of the study (Shadrach et al., 2021). GO category of the biological process showed these TFs mainly involved in myeloid cell differentiation and homeostasis (*Spi1*, *Irf8*, etc), regulation of angiogenesis (12 TFs, *Runx1*, *Hif1a*, *Xbp1*, *Stat3*, etc), neurogenesis (*Cux1*, *Nkx6-2*, *Hif1a*, *Myc*, *Sox11*, *Etv5*, etc), and gliogenesis (*Myc*, *Sox11*, *Etv5*, *Nkx6-2*, etc), and ER unfolded protein response (*Atf3*, *Creb3*, *Xbp1*, etc) (Table S7).

To screen co-operated key TFs or other regulators (e.g. epigenetic modification-related genes), we performed regulatory network analysis using the SCENIC pipeline. Given a relatively high correlation in expression of DEGs between rat and mouse post-SNC (Figure 3A) and lacking *cis*-regulatory motifs for the rat, we inferred regulon (a regulator and its targets) activity based on mouse motif dataset (–500–100 bp) and then performed clustering analysis of connection specificity index (CSI) (Suo et al., 2018). The regulons could be divided into seven distinct modules and two modules (M4 and M7) were focused with pro-growth TFs hits, specifically M4 (*Atf3*, *Stat3*, *Myc*, *Jun*, *Smad1*, *Klf6*, and *Klf7*, Figure 4B). Master regulators of 16 regulons (M4) were robust DEGs, respectively (Figure 4C). GO enrichment showed M4 regulons were significantly enriched in terms related to cytoskeleton, neurogenesis, signaling transduction, inflammatory and immune response, and response to wounding (Table S8). Except for well-known regulators (*Atf3*, *Stat3*, *Jun*, etc) in M4, we also found TFs related to unfolded protein response (UPR) were enriched (*Atf3*, *Creb3*, and *Xbp1*). ER stress could be provoked by tissue injury. UPR is important for preserving ER proteostasis and consists of three branches (IRE1 α -XBP1, PERK-CHOP, and ATF6-SREBP) depending on their activation in either promoting protein folding or apoptotic process or sterol biosynthesis. We observed upregulation of *Xbp1* at 3 and 7 days post-SNC, but *Ern1* (also known as IRE1 α) showed no

significant difference. *Creb3*, a homolog with *Atf6*, could be retrogradely transported to the nucleus to regulate the UPR and cholesterol biosynthesis by binding with *Srebf1* or *Srebf2* (Ying et al., 2014). We found *Creb3* and *Srebf2* were co-occurred in M4 and robust upregulation at 3 and/or 7 days post-SNC. Besides, enrichment analysis of UPR-related terms showed PERK-mediated UPR was the most enriched from 1 to 7 days (Figure S11), but its downstream regulator (CHOP) has no significant difference. These results suggested *Creb3-Srebf2* pathway may be the predominant UPR in spinal motor neurons after PNI. We also found epigenetic modification-related regulators occurred in M4 (*Hdac2* and *Gadd45a*). "Chromatin remodeling" was significantly enriched at 3 and 7 days post-SNC (Figure S12). Strikingly, we found a chromatin-remodeling enzyme, *Apobec1*, a known DNA demethylation mediator, showed a dramatic increase at 3 (74.2-fold) and 7 days (60.5-fold) post-SNC. We also found other seven known DNA demethylation mediators (Weng et al., 2017) (*Tet3*, *Tet2*, *Gadd45a*, b, g, and *Apobec1* and 3, Figure S12) showed significant upregulation, specifically *Apobec1*, 3 and *Gadd45g*. *Apobec1* was solely expressed in microglia and knock-down of *Apobec1* led to aberrant myelination, increased inflammation, and lysosomal anomalies in mouse brain (Cole et al., 2017). Thus, dramatic upregulation of *Apobec1* may be beneficial for axon regeneration by maintaining a balance between the homeostatic and activated immune functions of microglia.

We also employed the Algorithm for the Reconstruction of Accurate Cellular Network (ARACNe) which could identify transcriptional interaction based on information-theoretic method on a large gene expression data (Margolin et al., 2006). We analyzed 1,595 TFs or genes with "DNA-binding transcription factor activity" and then employed ssMARINA to infer candidate master regulators (MRs) post-SNC (Aytes et al., 2014). We focused on activated MRs at 1 day which is critical on axon regeneration as we extensively discussed above. MARINA identified 41 candidate MRs (FDR <0.05, Table S9) at 1 day and top 10 ranked MRs including *Atf3*, *Klf6*, *Myc*, and *Sox11*, which were well-known pro-regenerative MRs in axon growth (Venkatesh et al., 2021) (Figure 4D). We found 13 out of 20 co-operated regulators in M4 were also present in MRs identified by MARINA (Figure 4E). Specifically, we noticed the top MR, *Arid5a* (AT-Rich interaction domain 5A), has dual roles as TF and RNA-binding protein, that previously reported induction by inflammation stimulation to translocate from nucleus to the cytoplasm, stabilizes the expression of inflammatory genes, such as *Il6* and *Stat3* (Masuda et al., 2013; Nyati et al., 2019). We found the expression of *Arid5a* was only significantly upregulated at state 2 and/or state 3 (1 day: 7.69-fold at state 3 and 9.61-fold at state 2; 3 days: 8.58-fold; 7 days: 10-fold, Figure 4F), showing the activation at 1 day. Additionally, we found *Arid5a* was one target of the MR, *Atf3*, which presented a binding site of *Atf3* motif within 1k bp from 5' upstream of transcription start site (Figure 4G) and was also supported by ChIP data (Gilchrist et al., 2006). We found ARID5A mostly expressed in spinal neurons and obviously upregulated in injured MNs at 1 day and gradually increased at 3 and 7 days post-injury, specific in the cytoplasm (Figure 4H). This trend was consistent with our sequencing data. Furthermore, reanalysis of a single-cell sequencing (Hu et al., 2016) of sensory neurons and transcriptome datasets (Rozenbaum et al., 2018) of sensory neurons and glia in mouse DRG after sciatic nerve injury also showed robust upregulation of *Arid5a* in injured sensory neurons (Figure S14), which was consistent with the findings in MNs. These evidences indicated upregulation of *Arid5a* was conserved in injured neurons against sciatic nerve injury. Knockdown of *Arid5a* in primary sensory neurons showed a significant reduction of total neurite length *in vitro* (Figures 4I and S15, $p < 0.001$), suggesting its new role in axon regeneration. Reanalysis of recently released RNA-seq dataset of mouse embryonic fibroblast cells (MEFs), could be induced into neuronal cells (Treutlein et al., 2016) from wild type or *Arid5a*^{-/-} with or without IL6 stimulation (Nyati et al., 2021) showed that 987 genes (873 genes were orthologs in rat) were significantly downregulated in *Arid5a*^{-/-} while less change induced by IL6 compared to the wild type (Figure S13). We termed these genes as *Arid5a*-dependent and the top 20 downregulated genes included *Stmn2* (also known as SCG10, a marker of regenerating axons and regulation of microtubule dynamics). GO enrichment of *Arid5a*-dependent genes showed the term "regulation of neuron projection development" was significantly enriched, including genes related to axon regeneration (*Gap43*, *Stmn2*, and *Stmn4*, Figure S13). GSEA enrichment of *Arid5a*-dependent genes in our data showed significant enrichment in state 2 (injury and regenerating state) from 3 to 7 days post-injury (Figure 4J).

An axon regeneration-associated co-expressed module

Next, we performed weighted co-expression analysis (WGCNA) to detect regeneration-associated modules and identified 19 distinct modules (Figure 5A). We found the "turquoise" (1,705 genes, Table S10) showed a significant correlation with state 2 from 3 to 7 days based on the module eigengene (adjust p -value < 0.05, Figure 5A). Genes in "turquoise" showed a high expression in state 2 (Figure 5B). We compared this module with the "regenerative" module (413 genes) in DRG identified by

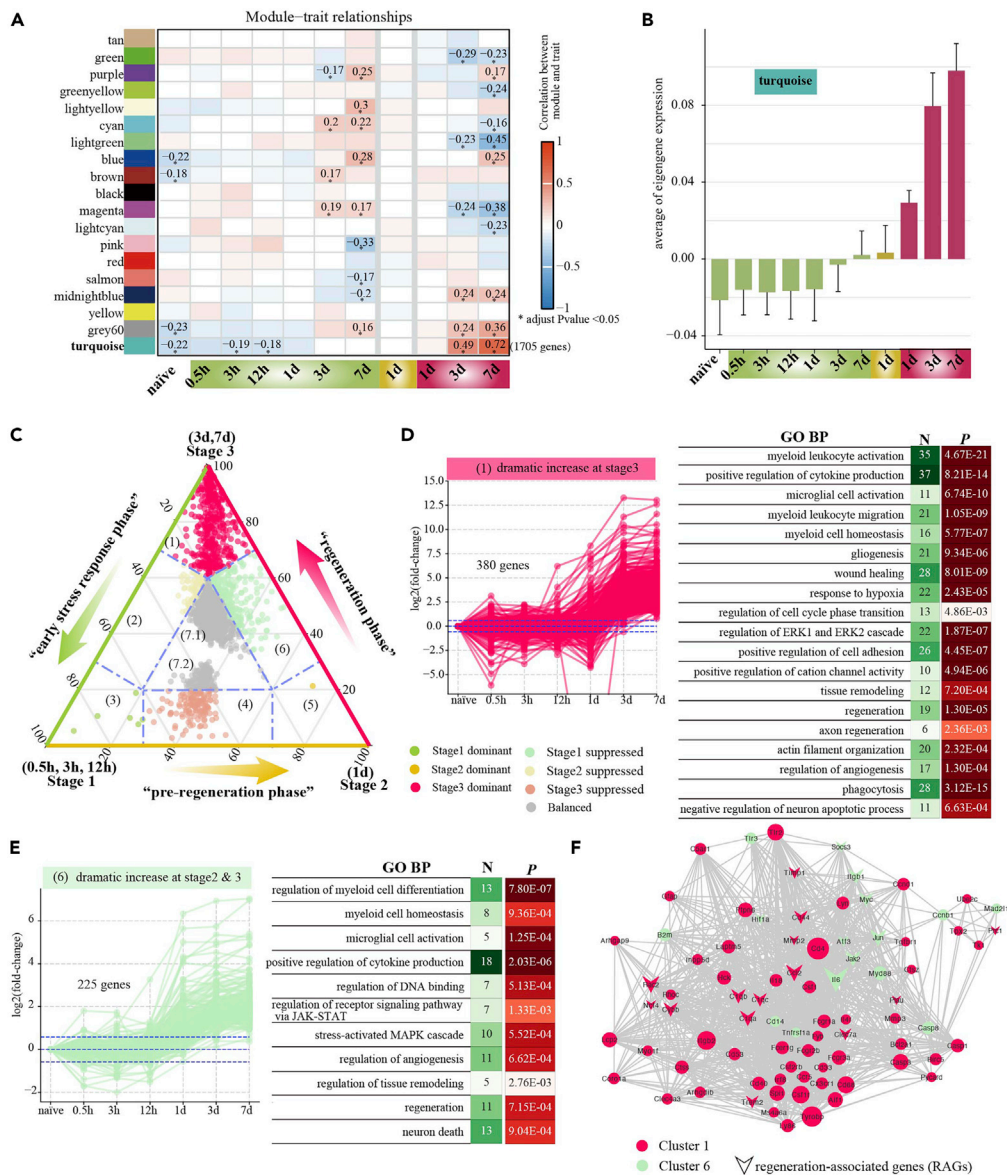


Figure 5. A module potentially related to axonal injury and regeneration was revealed by co-expression analysis

(A) Relationship between modules and traits (injured time points with different states here). Only correlation with significant (adjust p-value ≤ 0.05) was shown (*).
 (B) Gene expression pattern of the “turquoise” module based on the module eigengene values.
 (C) Ternary plots showed relative expression abundance of 1705 triads. Each circle represents a gene triad with Stage 1, 2, and 3 coordinates consisting of the relative contribution of each gene to the overall triad expression. Seven categories were assigned based on triad values.
 (D and E) Gene expression trends of cluster 1 (D, left) and cluster 6 (E, left) and GO enrichment of biological processes. N indicates gene number and p indicates p-value.
 (F) Highly connected protein-protein interaction of genes from clusters 1 and 6. Nodes with degrees ≥ 20 were shown.

Chandran et al. (2016) and 36.9% were also present in our “turquoise” module, such as *Ccl2*, *Ccl7*, *Atf3*, *Cd44*, *Il6*, and *Jun*. Next, we used a ternary plot-based method to explore expression patterns of genes in the “turquoise” module. Genes in the “turquoise” module were classified into seven major clusters and then focused on two clusters with upregulation after SNC (cluster 1 and 6, Figure 5C). We found most RAG genes were present in cluster 1 (*Ngfr*, *Pdlim1*, *Gap43*, *Mmp2*, *Tspo*, etc) and cluster 6 (*Atf3*, *Il6*, *Myc*, *Jun*, *Socs3*, *Sox11*, *Hif1a*, *Klf6*, etc). GO enrichment analysis of genes in these two clusters showed

inflammation and immune response were the most enriched categories, such as “microglial cell activation”, “neuroinflammatory response”, and “positive regulation of cytokine production” (Tables S11 and S12), suggesting that sterile inflammation induced by injury is closely related with axon regeneration. In addition, we found TF-related terms (regulation of DNA binding) were significant enrichment in cluster r6, including *Bcl3*, *Jak2*, *Jun*, *Myc*, and *Sox11*, supporting our above hypothesis that pro-growth TFs were activated as early as 1 day post-SNC. In addition, pro-regenerative pathways, such as MAPK cascade was also enriched at 1 day post-SNC. Genes related with “actin filament organization” and “axon regeneration” were enriched at stage 3 (namely 3 days and 7 days), such as *Gap43*, *Tspo*, and *Rac2*, suggesting that axon regeneration was mainly initiated as early as 3 days.

Next, we inferred the potential protein-protein interaction (PPI) network of genes in clusters 1 and 6. A highly connected PPI network showed the importance of proteins related injured neuron-microglia/macrophage crosstalk (*Il6*, *Csf1*, *Ccl2*, and *Csf1r*) with high connection and dramatic transcriptional changes (degree ≥ 20 , Figure 5F). We found genes involved in microglia response (activation and proliferation) were present in the network, such as *Trem2*, *Tyrobp*, *Spi1*, *Irf8*, *Cx3cr1*, and *Aif1*. We also found the pro-regenerative TFs, *Jun*, *Atf3*, *Myc*, and *Hif1a*, were present in the network. Potential genes identified here will provide important candidates for further drug development for PNS treatment.

DISCUSSION

Intrinsic regeneration capacity and exogenic supportive microenvironment greatly contribute to successful axon regeneration, specific immune system (Scheib and Hoke, 2013). Taking advantage of LCM-seq featured with collecting the target cell and its microecology *in situ* and in-depth sequencing, enabled us to obtain temporal-spatial profiles of MNs and the *in vivo* interactions between injured MNs and non-neuronal cells within the context of axon injury and regeneration through thorough molecule analysis. To our current knowledge, this new dataset was the first, massive and in-depth sequencing at approximate single-MN resolution. To facilitate exploration by other researchers, our data are easily searchable at MNniches-seq.

In this study, we established dynamic expression of MN niches at hours (0.5, 3, and 12 h) or days (1, 3, and 7 days) following SNC and the naive and divided into three response stages via thorough molecules analysis (0.5–12 h: early stress response phase; 1 day: pre-regeneration phase; 3~7 days: regeneration phase, Figure 6). Comparison of DEGs at 7 days post-SNC between our study and the study (Shadrach et al., 2021) demonstrated significant correlations and together with immunohistochemical validation indicating reproducibility and accuracy of our data. Based on clustering analysis and *Atf3*, we could well discriminate samples with injured MNs or “intact” MNs at 1, 3, and 7 days, which were supported by immunostaining results that ATF3-positive MNs present as early as 1 day of part MNs. Besides, the estimated injured ratios were in accordance with the estimation in previous studies (Holland et al., 2019; Renthall et al., 2020). Two cell states (state 1: “intact” and state 2: “injury”) were distinguished at 3 and 7 days, which was perfectly supported by both *Atf3* expression and clustering results. Strikingly, in addition to “intact” and “injury” states, we also found an additional state (defined as state 3, 26.5% of cells at 1 day, Figure 2A) that transient dramatic up-regulation of *Atf3* indicating injury which represents predominate state at 1 day, while “injury” states were rarely captured (defined as state 2, 6.1%), which suggested that state 3 at 1 day was intermediate transition states and rarely dissected MNs in state 2 may be explained by individual fast growth MNs. Considering the small number of MNs in state 2 at 1 day, we majorly focused on state 3 at 1 day. DEG analysis compared with the naive showed clear and distinct gene profiles after sample separation suggested that this could well reflect cell states at 1, 3, and 7 days post-SNC. Evidences of regenerating axon marker, RAGs, enrichment of multiple pro-regenerative pathways showed early pro-regenerative and master regulators (e.g., *Atf3*, *Jun*, *Sox11*, *Smad1*, and *Stat3*) were activated as early as 1 day while regenerating RAGs (e.g. *Gap43* and *Sprr1a*) were activated in samples with injured MNs at 3 and 7 days, suggesting “pre-regenerative” at 1 day and “regenerative” at 3 and 7 days. The small number of DEGs at 0.5–12 h and significant increase of DEGs at 1 day (state 2 and state 3) and dramatic increase of DEGs at 3 and 7 days (state 2) suggest 1 day post-injury is a key point. Though the increase of DEG number in state 1 at 3 and 7 days, inflammation and immune response-related genes were the most enriched which provide a vital control to explore crucial genes that contributed to the injury response and regeneration in injured MNs.

By comparison with samples containing the naive and corresponding “intact” MNs, we found genes involved in crosstalk between injured neuron-microglia/infiltrated macrophage was ranked at the top of

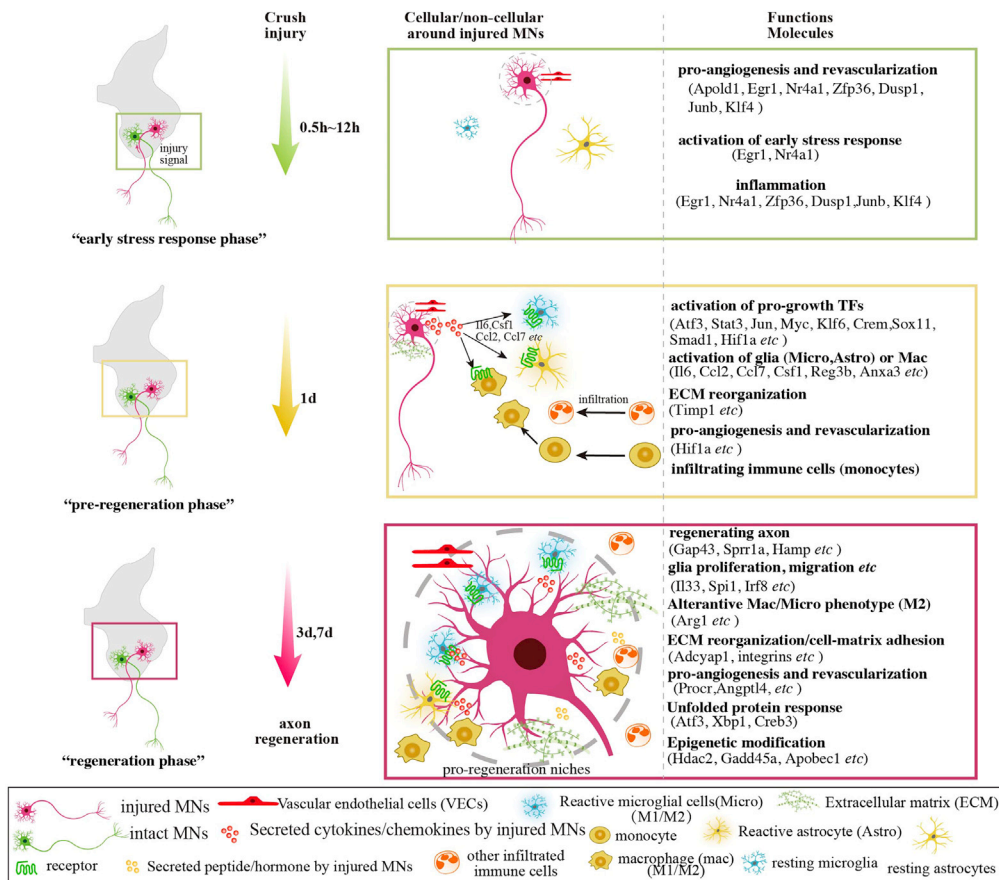


Figure 6. Schema of three response phases of injured motoneuron soma post-SNC

1d was a key point in axon regeneration that activated essential pro-regrowth-related TFs and non-neuronal cells. High dynamic of injured motoneurons niches occurred at regeneration phase (3 and 7 days) with high cellular heterogeneity and molecules involved in regeneration.

DEGs, such as neuronal *Il6*, *Ccl2*, *Ccl7*, *Csf1*, and *Reg3b*, which was not different between samples with “intact” MNs and the naive. Significant upregulation of microglia/macrophage markers, e.g., *Aif1* (IBA1), *Lyz2*, *Clec7a*, *Trem2*, *Tyrobp*, *Adgre1*, *Itgam*, *Ly86*, and *C1qa*, in samples with “injury” MNs at 3 and 7 days compared to that with the naive and “intact” MNs, suggested closely crosstalk between injured neuron-microglia, which was also present in the DEGs of the study (Shadrach et al., 2021). Our immunostaining of ANXA3 and IBA1 demonstrated that microglia almost adhered around injured MNs at 7 days post-SNC, which was in accordance with our sequenced result and other study (Rotterman and Alvarez, 2020). Single-cell sequencing of the injured spinal cord showed the significant microglia subtypes transition from homeostatic microglia subtype to disease-associated microglia subtype at 1 day then revert back to a more homeostatic state (3 and 7 days) (Milich et al., 2021), suggesting microglia/macrophage contribute the most to the dynamic microenvironment. Activated microglia/macrophage released neurotrophic factors but also produced pro-inflammatory factors contributing to phagocytose cell debris for promoting regeneration (Scheib and Hoke, 2013). M2 phenotype of microglia/macrophage could be pro-regenerative by releasing anti-inflammation factors (Scheib and Hoke, 2013). We found significant upregulation of genes promoting microglia/macrophage phenotype transition, e.g., *Arg1*. In addition to microglia/macrophage, we also found robust upregulation markers of endothelial cells (*Procr*), astrocyte (*Gfap*). We found enriched genes involved in angiogenesis included *Hif1a*, *Cd40*, *Grn*, and *Angptl4*. In non-cellular, we also found the dynamic extracellular matrix organization reflected by DEGs involved cells-matrix (integrins, such as *Itgam* and *Itgb2*). In addition to releasing factors mediating the interaction of neuron-cells, neuron-matrix, and cells-cells for permissive microenvironment, injured MNs also activate intrinsic pro-regenerative TFs, such as *Atf3*, *Sox11*, *Jun*, *Smad1*, and *Myc*. Besides, injured MNs released

pro-regenerative peptides/hormones and growth factors/receptors, such as *Vip*, *Adcyap1*, *Ngfr*, *Grn*, and anti-apoptotic proteins (e.g., *Gadd45a*) and upregulate axon regrowth factor (e.g., *Gap43*, *Sprr1a*, *Rac2*, and *Pdlim1*).

We also deeply explored potential regulators, including TF and epigenetic modification (e.g., demethylation and acetylation). We identified potential co-operated regulators including well-known TFs (*Klf6*, *Klf7*, *Atf3*, *Myc*, *Stat3*, and *Smad1*) and unfolded protein response (*Atf3*, *Creb3*, and *Xbp1*) and epigenetic modification (*Hdac2* and *Gadd45a*). Except for the well-known TFs supported by MARAINa analysis, we also highlighted a candidate master regulator, *Arid5a*. Its roles in the regulation of chondrocyte-specific transcription (acting as a transcription factor) and inflammatory processes (acting as an RNA-binding protein) by stabilizing inflammatory mRNA transcripts were described (Amano et al., 2011; Masuda et al., 2013). However, studies of *Arid5a* expression and potential roles during axonal injury and regeneration were blank. We found significant upregulation of *Arid5a* in samples with injured MNs both at transcriptional and protein level post-SNC (Figures 4G and 4I). This was also supported by significant upregulation of translating *Arid5a* level in injured MNs compared to the control (Shadrach et al., 2021). Knockdown of *Arid5a* in primary sensory neurons suggested its potential new role in axon growth (Figure 4I). Additionally, *Arid5a* is also a potential target of the pro-regenerative regulator, *Atf3*, and showed a high correlation in expression (Figure 4A, Pearson's cor: 0.98). Reanalysis of *Arid5a* knockout (KO) dataset of mouse embryonic fibroblast cell showed axon growth-related genes were largely downregulated in *Arid5a* KO group and geneset enrichment of these downregulated genes showed significantly enriched at samples with injured and regenerating MNs (Figure 4J), indicating the importance of *Arid5a* in axon regeneration. Recently, a study of brain ischemic injury showed that overexpression of ARID5A in primary cortical neurons elicited neuroprotection against oxygen-glucose deprivation injury (Cai et al., 2019). Taken together, we suspected that upregulation of *Arid5a* in samples with injured neurons may promote axon regeneration and might be an undescribed role of the less studied function of *Arid5a* in PNI, and its mechanism required further investigation.

In conclusion, we firstly present the landscape of cellular and molecular interactions between injured and regenerating MNs and its permissive microenvironment *in situ* during the complex first seven days post-injury using LCM-seq. Specifically, distinguishing and comparison of "intact" and "injury" MN niches at the similar environment yielding numerous injury-induced and pro-regenerative genes, though most of their function in promoting axon regeneration of MNs remains to be explored. Through thorough molecular analysis, we resolved three response stages and molecular characteristics of the injured MN and its microenvironment and highlighted critical regulators, for instance, *Arid5a*. This study not only provides gene regulation patterns for regeneration of the injured spinal motoneuron and its dynamic microenvironment but also gains insights into potential new targets for the treatment of motoneuron dysfunction and gives the genetic basis for development of tissue engineering and regenerative medicine.

Limitations of the study

Two major limitations exist in this study. First, acting as a method for single-cell isolation, LCM has a major disadvantage that inevitably contains neighboring cells or non-cells of the target cell. Thus, the expression profile presented here not only contained the motoneuron but also mixed with its microecology, including other cells or non-cells. Second, for hypothetical roles in axonal injury and regeneration and underlying mechanisms of candidate genes, for example, *Arid5a*, further functional experiments *in vitro* and *in vivo* are required.

STAR★METHODS

Detailed methods are provided in the online version of this paper and include the following:

- KEY RESOURCES TABLE
- RESOURCE AVAILABILITY
 - Lead contact
 - Materials availability
 - Data and code availability
- EXPERIMENTAL MODEL AND SUBJECT DETAILS
 - Animals
- METHOD DETAILS

- Nerve crush
- Tissue preparation and rapid staining of MNs before laser capture microscopy
- Laser capture microscopy
- Smart-seq2 procedure for cDNA library preparation and sequencing
- Immunofluorescence histochemistry
- DRG neuron culture and siRNA transfection
- **QUANTIFICATION AND DATA ANALYSIS**
 - RNA-seq mapping, quantification, and clustering analysis
 - Differential expression analysis
 - Transcriptional factors (TFs) analysis
 - Gene set enrichment analysis
 - WGCNA co-expression analysis
 - Functional enrichment analysis
 - Public dataset analysis

SUPPLEMENTAL INFORMATION

Supplemental information can be found online at <https://doi.org/10.1016/j.isci.2022.104917>.

ACKNOWLEDGMENTS

This work was supported by the National Natural Science Foundation of China (Grant No. 31730031, 32130060), the Natural Science Foundation of Jiangsu Province (BK20202013), the Jiangsu Provincial Key Medical Center, and Priority Academic Program Development of Jiangsu Higher Education Institutions (PAPD) and the Shuangchuang Doctor program of Jiangsu Province (Grant No. JSSCBS20211127).

AUTHOR CONTRIBUTIONS

X.S.G. and J.Y. designed the experiments. Y.Z., J.Y., X.D.L., Z.F.C., J.C., and T.Z. collected samples and performed experiments. L.X., J.Y., and Y.Z. performed the computational analysis. L.X., J.Y., Y.Z., and X.S.G. wrote the manuscript.

DECLARATION OF INTERESTS

The authors declare no conflicts of interest.

Received: March 24, 2022

Revised: July 10, 2022

Accepted: August 8, 2022

Published: September 16, 2022

REFERENCES

- Aguila, J., Cheng, S., Kee, N., Cao, M., Wang, M., Deng, Q., and Hedlund, E. (2021). Spatial RNA sequencing identifies robust markers of vulnerable and resistant human midbrain dopamine neurons and their expression in Parkinson's disease. *Front. Mol. Neurosci.* *14*, 699562. <https://doi.org/10.3389/fnmol.2021.699562>.
- Aibar, S., González-Blas, C.B., Moerman, T., Huynh-Thu, V.A., Imrichova, H., Hulselmans, G., Rambow, F., Marine, J.C., Geurts, P., Aerts, J., et al. (2017). SCENIC: single-cell regulatory network inference and clustering. *Nat. Methods* *14*, 1083–1086. <https://doi.org/10.1038/nmeth.4463>.
- Amano, K., Hata, K., Muramatsu, S., Wakabayashi, M., Takigawa, Y., Ono, K., Nakanishi, M., Takashima, R., Kogo, M., Matsuda, A., et al. (2011). Arid5a cooperates with Sox9 to stimulate chondrocyte-specific transcription. *Mol. Biol. Cell* *22*, 1300–1311. <https://doi.org/10.1091/mbc.E10-07-0566>.
- Anders, S., Pyl, P.T., and Huber, W. (2015). HTSeq—a Python framework to work with high-throughput sequencing data. *Bioinformatics* *31*, 166–169. <https://doi.org/10.1093/bioinformatics/btu638>.
- Avraham, O., Deng, P.Y., Jones, S., Kuruvilla, R., Semenkovich, C.F., Klyachko, V.A., and Cavalli, V. (2020). Satellite glial cells promote regenerative growth in sensory neurons. *Nat. Commun.* *11*, 4891. <https://doi.org/10.1038/s41467-020-18642-y>.
- Aytes, A., Mitrofanova, A., Lefebvre, C., Alvarez, M.J., Castillo-Martin, M., Zheng, T., Eastham, J.A., Gopalan, A., Pienta, K.J., Shen, M.M., et al. (2014). Cross-species regulatory network analysis identifies a synergistic interaction between FOXM1 and CENPF that drives prostate cancer malignancy. *Cancer Cell* *25*, 638–651. <https://doi.org/10.1016/j.ccr.2014.03.017>.
- Baskozos, G., Sandy-Hindmarch, O., Clark, A.J., Windsor, K., Karlsson, P., Weir, G.A., McDermott, L.A., Burchall, J., Wiberg, A., Furniss, D., et al. (2020). Molecular and cellular correlates of human nerve regeneration: ADCYAP1/PACAP enhance nerve outgrowth. *Brain* *143*, 2009–2026. <https://doi.org/10.1093/brain/awaa163>.
- Blum, J.A., Klemm, S., Shadrach, J.L., Gattenplan, K.A., Nakayama, L., Kathiria, A., Hoang, P.T., Gautier, O., Kaltschmidt, J.A., Greenleaf, W.J., and Gitler, A.D. (2021). Single-cell transcriptomic analysis of the adult mouse spinal cord reveals molecular diversity of autonomic and skeletal motor neurons. *Nat. Neurosci.* *24*, 572–583. <https://doi.org/10.1038/s41593-020-00795-0>.
- Butler, A., Hoffman, P., Smibert, P., Papalexis, E., and Satija, R. (2018). Integrating single-cell transcriptomic data across different conditions,

- technologies, and species. *Nat. Biotechnol.* 36, 411–420. <https://doi.org/10.1038/nbt.4096>.
- Cahoy, J.D., Emery, B., Kaushal, A., Foo, L.C., Zamanian, J.L., Christopherson, K.S., Xing, Y., Lubischer, J.L., Krieg, P.A., Krupenko, S.A., et al. (2008). A transcriptome database for astrocytes, neurons, and oligodendrocytes: a new resource for understanding brain development and function. *J. Neurosci.* 28, 264–278. <https://doi.org/10.1523/JNEUROSCI.4178-07.2008>.
- Cai, M., Zhu, Y., Li, Z., Josephs-Spaulding, J., Zhou, Y., Hu, Y., Chen, H., Liu, Y., He, W., and Zhang, J. (2019). Profiling the gene expression and DNA methylation in the mouse brain after ischemic preconditioning. *Neuroscience* 406, 249–261. <https://doi.org/10.1016/j.neuroscience.2019.03.023>.
- Chandran, V., Coppola, G., Nawabi, H., Omura, T., Versano, R., Huebner, E.A., Zhang, A., Costigan, M., Yekkirala, A., Barrett, L., et al. (2016). A systems-level analysis of the peripheral nerve intrinsic axonal growth program. *Neuron* 89, 956–970. <https://doi.org/10.1016/j.neuron.2016.01.034>.
- Cho, Y., Shin, J.E., Ewan, E.E., Oh, Y.M., Pita-Thomas, W., and Cavalli, V. (2015). Activating injury-responsive genes with hypoxia enhances axon regeneration through neuronal HIF-1 α . *Neuron* 88, 720–734. <https://doi.org/10.1016/j.neuron.2015.09.050>.
- Cole, D.C., Chung, Y., Gagnidze, K., Hajdarovic, K.H., Rayon-Estrada, V., Harjanto, D., Bigio, B., Gal-Toth, J., Milner, T.A., McEwen, B.S., et al. (2017). Loss of APOBEC1 RNA-editing function in microglia exacerbates age-related CNS pathophysiology. *Proc. Natl. Acad. Sci. USA* 114, 13272–13277. <https://doi.org/10.1073/pnas.1710493114>.
- Fornes, O., Castro-Mondragon, J.A., Khan, A., van der Lee, R., Zhang, X., Richmond, P.A., Modi, B.P., Correard, S., Gheorghe, M., Baranašić, D., et al. (2020). JASPAR 2020: update of the open-access database of transcription factor binding profiles. *Nucleic Acids Res.* 48, D87–D92. <https://doi.org/10.1093/nar/gkz1001>.
- Gadani, S.P., Walsh, J.T., Lukens, J.R., and Kipnis, J. (2015a). Dealing with danger in the CNS: the response of the immune system to injury. *Neuron* 87, 47–62. <https://doi.org/10.1016/j.neuron.2015.05.019>.
- Gadani, S.P., Walsh, J.T., Smirnov, I., Zheng, J., and Kipnis, J. (2015b). The glia-derived alarmin IL-33 orchestrates the immune response and promotes recovery following CNS injury. *Neuron* 85, 703–709. <https://doi.org/10.1016/j.neuron.2015.01.013>.
- Gilchrist, M., Thorsson, V., Li, B., Rust, A.G., Korb, M., Roach, J.C., Kennedy, K., Hai, T., Bolouri, H., and Aderem, A. (2006). Systems biology approaches identify ATF3 as a negative regulator of Toll-like receptor 4. *Nature* 441, 173–178. <https://doi.org/10.1038/nature04768>.
- Grant, C.E., Bailey, T.L., and Noble, W.S. (2011). FIMO: scanning for occurrences of a given motif. *Bioinformatics* 27, 1017–1018. <https://doi.org/10.1093/bioinformatics/btr064>.
- Guaiquil, V.H., Pan, Z., Karagianni, N., Fukuoka, S., Alegre, G., and Rosenblatt, M.I. (2014). VEGF-B selectively regenerates injured peripheral neurons and restores sensory and trophic functions. *Proc. Natl. Acad. Sci. USA* 111, 17272–17277. <https://doi.org/10.1073/pnas.1407227111>.
- Hamilton, N.E., and Ferry, M. (2018). Ggtern: ternary diagrams using ggplot2. *J. Stat. Softw.* 87, 1–17. <https://doi.org/10.18637/jss.v087.c03>.
- Harashima, M., Harada, K., Ito, Y., Hyuga, M., Seki, T., Ariga, T., Yamaguchi, T., and Niimi, S. (2008). Annexin A3 expression increases in hepatocytes and is regulated by hepatocyte growth factor in rat liver regeneration. *J. Biochem.* 143, 537–545. <https://doi.org/10.1093/jb/mvm248>.
- Holland, S.D., Ramer, L.M., McMahon, S.B., Denk, F., and Ramer, M.S. (2019). An ATF3-CreERT2 knock-in mouse for axotomy-induced genetic editing: proof of principle. *eNeuro* 6, ENEURO.0025-19.2019. <https://doi.org/10.1523/ENEURO.0025-19.2019>.
- Hu, G., Huang, K., Hu, Y., Du, G., Xue, Z., Zhu, X., and Fan, G. (2016). Single-cell RNA-seq reveals distinct injury responses in different types of DRG sensory neurons. *Sci. Rep.* 6, 31851. <https://doi.org/10.1038/srep31851>.
- Inoue, T., Kohro, T., Tanaka, T., Kanki, Y., Li, G., Poh, H.M., Mimura, I., Kobayashi, M., Taguchi, A., Maejima, T., et al. (2014). Cross-enhancement of ANGPTL4 transcription by HIF1 α and PPAR β /delta is the result of the conformational proximity of two response elements. *Genome Biol.* 15, R63. <https://doi.org/10.1186/gb-2014-15-4-r63>.
- Kim, D., Langmead, B., and Salzberg, S.L. (2015). HISAT: a fast spliced aligner with low memory requirements. *Nat. Methods* 12, 357–360. <https://doi.org/10.1038/nmeth.3317>.
- Kwon, M.J., Shin, H.Y., Cui, Y., Kim, H., Thi, A.H.L., Choi, J.Y., Kim, E.Y., Hwang, D.H., and Kim, B.G. (2015). CCL2 mediates neuron-macrophage interactions to drive proregenerative macrophage activation following preconditioning injury. *J. Neurosci.* 35, 15934–15947. <https://doi.org/10.1523/JNEUROSCI.1924-15.2015>.
- Langfelder, P., and Horvath, S. (2008). WGCNA: an R package for weighted correlation network analysis. *BMC Bioinformatics* 9, 559. <https://doi.org/10.1186/1471-2105-9-559>.
- Lee, S.Y., Kim, J.M., Cho, S.Y., Kim, H.S., Shin, H.S., Jeon, J.Y., Kausar, R., Jeong, S.Y., Lee, Y.S., and Lee, M.A. (2014). TIMP-1 modulates chemotaxis of human neural stem cells through CD63 and integrin signalling. *Biochem. J.* 459, 565–576. <https://doi.org/10.1042/BJ20131119>.
- Lei, W.L., Xing, S.G., Deng, C.Y., Ju, X.C., Jiang, X.Y., and Luo, Z.G. (2012). Laminin/ β 1 integrin signal triggers axon formation by promoting microtubule assembly and stabilization. *Cell Res.* 22, 954–972. <https://doi.org/10.1038/cr.2012.40>.
- Li, J., Shi, H., Liu, H., Dong, F., Liu, Z., Lu, Y., Chen, L., Bao, L., and Zhang, X. (2020a). Nerve injury-induced neuronal PAP-I maintains neuropathic pain by activating spinal microglia. *J. Neurosci.* 40, 297–310. <https://doi.org/10.1523/JNEUROSCI.1414-19.2019>.
- Li, R., Li, D.H., Zhang, H.Y., Wang, J., Li, X.K., and Xiao, J. (2020b). Growth factors-based therapeutic strategies and their underlying signaling mechanisms for peripheral nerve regeneration. *Acta Pharmacol. Sin.* 41, 1289–1300. <https://doi.org/10.1038/s41401-019-0338-1>.
- Love, M.I., Huber, W., and Anders, S. (2014). Moderated estimation of fold change and dispersion for RNA-seq data with DESeq2. *Genome Biol.* 15, 550. <https://doi.org/10.1186/s13059-014-0550-8>.
- Margolin, A.A., Nemenman, I., Basso, K., Wiggins, C., Stolovitzky, G., Dalla Favera, R., and Califano, A. (2006). ARACNE: an algorithm for the reconstruction of gene regulatory networks in a mammalian cellular context. *BMC Bioinformatics* 7. <https://doi.org/10.1186/1471-2105-7-S1-S7>.
- Masuda, K., Ripley, B., Nishimura, R., Mino, T., Takeuchi, O., Shioi, G., Kiyonari, H., and Kishimoto, T. (2013). Arid5a controls IL-6 mRNA stability, which contributes to elevation of IL-6 level in vivo. *Proc. Natl. Acad. Sci. USA* 110, 9409–9414. <https://doi.org/10.1073/pnas.1307419110>.
- Meijering, E., Jacob, M., Sarrja, J.C.F., Steiner, P., Hirling, H., and Unser, M. (2004). Design and validation of a tool for neurite tracing and analysis in fluorescence microscopy images. *Cytometry A* 58, 167–176.
- Milich, L.M., Choi, J.S., Ryan, C., Cerqueira, S.R., Benavides, S., Yahn, S.L., Tsoufas, P., and Lee, J.K. (2021). Single-cell analysis of the cellular heterogeneity and interactions in the injured mouse spinal cord. *J. Exp. Med.* 218, e20210040. <https://doi.org/10.1084/jem.20210040>.
- Namikawa, K., Fukushima, M., Murakami, K., Suzuki, A., Takasawa, S., Okamoto, H., and Kiyama, H. (2005). Expression of Reg/PAP family members during motor nerve regeneration in rat. *Biochem. Biophys. Res. Commun.* 332, 126–134. <https://doi.org/10.1016/j.bbrc.2005.04.105>.
- Newman, A.M., Liu, C.L., Green, M.R., Gentles, A.J., Feng, W., Xu, Y., Hoang, C.D., Diehn, M., and Alizadeh, A.A. (2015). Robust enumeration of cell subsets from tissue expression profiles. *Nat. Methods* 12, 453–457. <https://doi.org/10.1038/nmeth.3337>.
- Nichterwitz, S., Chen, G., Aguila Benitez, J., Yilmaz, M., Storrall, H., Cao, M., Sandberg, R., Deng, Q., and Hedlund, E. (2016). Laser capture microscopy coupled with Smart-seq2 for precise spatial transcriptomic profiling. *Nat. Commun.* 7, 12139. <https://doi.org/10.1038/ncomms12139>.
- Nichterwitz, S., Nijssen, J., Storrall, H., Schweingruber, C., Comley, L.H., Allodi, I., Lee, M.v.d., Deng, Q., Sandberg, R., and Hedlund, E. (2020). LCM-seq reveals unique transcriptional adaptation mechanisms of resistant neurons and identifies protective pathways in spinal muscular atrophy. *Genome Res.* 30, 1083–1096. <https://doi.org/10.1101/gr.265017.120>.
- Nyati, K.K., Agarwal, R.G., Sharma, P., and Kishimoto, T. (2019). Arid5a regulation and the roles of Arid5a in the inflammatory response and disease. *Front. Immunol.* 10, 2790. <https://doi.org/10.3389/fimmu.2019.02790>.
- Nyati, K.K., Hashimoto, S., Singh, S.K., Tekguc, M., Metwally, H., Liu, Y.C., Okuzaki, D., Gemechu,

- Y., Kang, S., and Kishimoto, T. (2021). The novel long noncoding RNA AU021063, induced by IL-6/Arid5a signaling, exacerbates breast cancer invasion and metastasis by stabilizing Trib3 and activating the Mek/Erk pathway. *Cancer Lett.* 520, 295–306. <https://doi.org/10.1016/j.canlet.2021.08.004>.
- Ogier, C., Creidy, R., Boucraut, J., Soloway, P.D., Khrestchatsky, M., and Rivera, S. (2005). Astrocyte reactivity to Fas activation is attenuated in TIMP-1 deficient mice, an in vitro study. *BMC Neurosci.* 6, 68. <https://doi.org/10.1186/1471-2202-6-68>.
- Park, J.E., Lee, D.H., Lee, J.A., Park, S.G., Kim, N.S., Park, B.C., and Cho, S. (2005). Annexin A3 is a potential angiogenic mediator. *Biochem. Biophys. Res. Commun.* 337, 1283–1287. <https://doi.org/10.1016/j.bbrc.2005.10.004>.
- Picelli, S., Björklund, Å.K., Faridani, O.R., Sagasser, S., Winberg, G., and Sandberg, R. (2013). Smart-seq2 for sensitive full-length transcriptome profiling in single cells. *Nat. Methods* 10, 1096–1098. <https://doi.org/10.1038/nmeth.2639>.
- R Core Team, R. (2018). *R: A Language and Environment for Statistical Computing* (R foundation for statistical computing Vienna).
- Ramírez-González, R.H., Borrill, P., Lang, D., Harrington, S.A., Brinton, J., Venturini, L., Davey, M., Jacobs, J., van Ex, F., Pasha, A., et al. (2018). The transcriptional landscape of polyploid wheat. *Science* 361, eaar6089. <https://doi.org/10.1126/science.aar6089>.
- Renthal, W., Tochitsky, I., Yang, L., Cheng, Y.C., Li, E., Kawaguchi, R., Geschwind, D.H., and Woolf, C.J. (2020). Transcriptional reprogramming of distinct peripheral sensory neuron subtypes after axonal injury. *Neuron* 108, 128–144.e9. <https://doi.org/10.1016/j.neuron.2020.07.026>.
- Rotterman, T.M., and Alvarez, F.J. (2020). Microglia dynamics and interactions with motoneurons axotomized after nerve injuries revealed by two-photon imaging. *Sci. Rep.* 10, 8648. <https://doi.org/10.1038/s41598-020-65363-9>.
- Roumazielles, L., Dokalis, N., Kaulich, E., and Lelievre, V. (2018). It is all about the support - the role of the extracellular matrix in regenerating axon guidance. *Cell Adh. Migr.* 12, 87–92. <https://doi.org/10.1080/19336918.2017.1291481>.
- Rozenbaum, M., Rajman, M., Rishal, I., Koppel, I., Koley, S., Medzihradsky, K.F., Oses-Prieto, J.A., Kawaguchi, R., Amieux, P.S., Burlingame, A.L., et al. (2018). Translatome regulation in neuronal injury and axon regrowth. *eNeuro* 5, ENEURO.0276-17.2018. <https://doi.org/10.1523/ENEURO.0276-17.2018>.
- Scheib, J., and Höke, A. (2013). Advances in peripheral nerve regeneration. *Nat. Rev. Neurol.* 9, 668–676. <https://doi.org/10.1038/nrneurol.2013.227>.
- Schneider, C.A., Rasband, W.S., and Eliceiri, K.W. (2012). NIH Image to ImageJ: 25 years of image analysis. *Nat. Methods* 9, 671–675. <https://doi.org/10.1038/nmeth.2089>.
- Shadrach, J.L., Stansberry, W.M., Milen, A.M., Ives, R.E., Fogarty, E.A., Antonellis, A., and Pierchala, B.A. (2021). Translational analysis of regenerating and degenerating spinal motor neurons in injury and ALS. *iScience* 24, 102700. <https://doi.org/10.1016/j.isci.2021.102700>.
- Shaked, I., Hanna, R.N., Shaked, H., Chodaczek, G., Nowyhed, H.N., Tweet, G., Tacke, R., Basat, A.B., Mikulski, Z., Togher, S., et al. (2015). Transcription factor Nr4a1 couples sympathetic and inflammatory cues in CNS-recruited macrophages to limit neuroinflammation. *Nat. Immunol.* 16, 1228–1234. <https://doi.org/10.1038/ni.3321>.
- Subramanian, A., Tamayo, P., Mootha, V.K., Mukherjee, S., Ebert, B.L., Gillette, M.A., Paulovich, A., Pomeroy, S.L., Golub, T.R., Lander, E.S., and Mesirov, J.P. (2005). Gene set enrichment analysis: a knowledge-based approach for interpreting genome-wide expression profiles. *Proc. Natl. Acad. Sci. USA* 102, 15545–15550. <https://doi.org/10.1073/pnas.0506580102>.
- Suo, S., Zhu, Q., Saadatpour, A., Fei, L., Guo, G., and Yuan, G.C. (2018). Revealing the critical regulators of cell identity in the mouse cell atlas. *Cell Rep.* 25, 1436–1445.e3. <https://doi.org/10.1016/j.celrep.2018.10.045>.
- Treutlein, B., Lee, Q.Y., Camp, J.G., Mall, M., Koh, W., Shariati, S.A.M., Sim, S., Neff, N.F., Skotheim, J.M., Wernig, M., and Quake, S.R. (2016). Dissecting direct reprogramming from fibroblast to neuron using single-cell RNA-seq. *Nature* 534, 391–395. <https://doi.org/10.1038/nature18323>.
- Trizzino, M., Zucco, A., Deliard, S., Wang, F., Barbieri, E., Veglia, F., Gabrilovich, D., and Gardini, A. (2021). EGR1 is a gatekeeper of inflammatory enhancers in human macrophages. *Sci. Adv.* 7, eaaz8836. <https://doi.org/10.1126/sciadv.aaz8836>.
- Tsujino, H., Kondo, E., Fukuoka, T., Dai, Y., Tokunaga, A., Miki, K., Yonenobu, K., Ochi, T., and Noguchi, K. (2000). Activating transcription factor 3 (ATF3) induction by axotomy in sensory and motoneurons: a novel neuronal marker of nerve injury. *Mol. Cell. Neurosci.* 15, 170–182. <https://doi.org/10.1006/mcne.1999.0814>.
- Venkatesh, I., Mehra, V., Wang, Z., Simpson, M.T., Eastwood, E., Chakraborty, A., Beine, Z., Gross, D., Cabahug, M., Olson, G., and Blackmore, M.G. (2021). Co-occupancy identifies transcription factor co-operation for axon growth. *Nat. Commun.* 12, 2555. <https://doi.org/10.1038/s41467-021-22828-3>.
- Vicuña, L., Strohlic, D.E., Latremoliere, A., Bali, K.K., Simonetti, M., Husainie, D., Prokosch, S., Riva, P., Griffin, R.S., Njoo, C., et al. (2015). The serine protease inhibitor SerpinA3N attenuates neuropathic pain by inhibiting T cell-derived leukocyte elastase. *Nat. Med.* 21, 518–523. <https://doi.org/10.1038/nm.3852>.
- Wang, K., Wang, S., Chen, Y., Wu, D., Hu, X., Lu, Y., Wang, L., Bao, L., Li, C., and Zhang, X. (2021). Single-cell transcriptomic analysis of somatosensory neurons uncovers temporal development of neuropathic pain. *Cell Res.* 31, 904–918. <https://doi.org/10.1038/s41422-021-00479-9>.
- Weng, Y.L., An, R., Cassin, J., Joseph, J., Mi, R., Wang, C., Zhong, C., Jin, S.G., Pfeifer, G.P., Bellacosa, A., et al. (2017). An intrinsic epigenetic barrier for functional axon regeneration. *Neuron* 94, 337–346.e6. <https://doi.org/10.1016/j.neuron.2017.03.034>.
- Woodley, P.K., Min, Q., Li, Y., Mulvey, N.F., Parkinson, D.B., and Dun, X.P. (2019). Distinct VIP and PACAP functions in the distal nerve stump during peripheral nerve regeneration. *Front. Neurosci.* 13, 1326. <https://doi.org/10.3389/fnins.2019.01326>.
- Ying, Z., Misra, V., and Verge, V.M.K. (2014). Sensing nerve injury at the axonal ER: activated Luman/CREB3 serves as a novel axonally synthesized retrograde regeneration signal. *Proc. Natl. Acad. Sci. USA* 111, 16142–16147. <https://doi.org/10.1073/pnas.1407462111>.
- Yu, L.M., Leipzig, N.D., and Shoichet, M.S. (2008). Promoting neuron adhesion and growth. *Mater. Today* 11, 36–43. [https://doi.org/10.1016/S1369-7021\(08\)70088-9](https://doi.org/10.1016/S1369-7021(08)70088-9).
- Yu, G., Wang, L.G., Han, Y., and He, Q.Y. (2012). clusterProfiler: an R package for comparing biological themes among gene clusters. *OMICS* 16, 284–287. <https://doi.org/10.1089/omi.2011.0118>.
- Yu, B., Yao, C., Wang, Y., Mao, S., Wang, Y., Wu, R., Feng, W., Chen, Y., Yang, J., Xue, C., et al. (2019). The landscape of gene expression and molecular regulation following spinal cord hemisection in rats. *Front. Mol. Neurosci.* 12, 287. <https://doi.org/10.3389/fnmol.2019.00287>.
- Zhang, Q.L., Liu, J., Lin, P.X., and Webster, H.D. (2002). Local administration of vasoactive intestinal peptide after nerve transection accelerates early myelination and growth of regenerating axons. *J. Peripher. Nerv. Syst.* 7, 118–127. <https://doi.org/10.1046/j.1529-8027.2002.02018.x>.
- Zhang, Z., Li, Z., Ma, Z., Deng, M., Xing, M., Wu, J., Jiang, S., Wang, Q., Guo, Q., and Zou, W. (2021). Annexin A3 as a marker protein for microglia in the central nervous system of rats. *Neural Plast.* 2021, 5575090. <https://doi.org/10.1155/2021/5575090>.

STAR★METHODS

KEY RESOURCES TABLE

REAGENT or RESOURCE	SOURCE	IDENTIFIER
Antibodies		
Anti-Choline Acetyltransferase antibody	Abcam	Cat# ab137349, RRID:AB_2754985
Anti-IBA1 antibody	Abcam	Cat# ab153696, RRID:AB_2889406
Anti-ARID5A antibody	Sigma-Aldrich	Cat# SAB2100148, RRID:AB_10598838
Annexin A3 antibody	Proteintech	Cat# 11804-1-AP, RRID:AB_2057455
ChAT Polyclonal antibody	Thermo Fisher Scientific	Cat# PA5-29653, RRID:AB_2547128
ATF3 antibody	Abcam	Cat# ab58668, RRID:AB_879578
NeuN antibody	Sigma-Aldrich	Cat# MAB377
Anti-Beta-III Tubulin antibody	R & D Systems	Cat# MAB1195, RRID:AB_357520
Chemicals, peptides, and recombinant proteins		
Diethyl pyrocarbonate	Sigma-Aldrich	Cat# D5758-100ML
Collagenase type I	Sigma-Aldrich	Cat# SCR103-250MG
Neurobasal-A medium	Thermo Fisher Scientific	Cat# 10888022
B-27 Supplement	Thermo Fisher Scientific	Cat# 17504044
L-Glutamine	Thermo Fisher Scientific	Cat# 25030149
Penicillin-Streptomycin	Beyotime	Cat# C0222
poly-L-lysine	Sigma-Aldrich	Cat# P4832
Trypsin-EDTA	Gibco	Cat# 25200-072
Critical commercial assays		
Lipofectamine RNAiMAX reverse transfection reagent	Thermo Fisher Scientific	Cat# 13778075
Deposited data		
Raw and analyzed data	This paper	CNGBdb: CNP0002605
Single-cell sequencing of mouse spinal cord after injury	Milich et al. (2021)	GEO: GSE162610
Bulk RNA-seq of rat spinal cord after injury	Yu et al. (2019)	NODE: OEP000369
Mouse embryonic fibroblast cells (MEFs) in wild-type or Arid5a knockout	Nyati et al. (2021)	GEO: GSE178250
Single-cell sequencing of mouse DRG neurons	Hu et al. (2016)	GEO: GSE71453
RiboTag data from DRG ganglia from Isl1-Cre and Dhh-Cre RiboTag mice	Rozenbaum et al. (2018)	GEO: GSE102316
RiboTag data of motoneurons from RiboTag; ChATCre mice	Shadrach et al. (2021)	GEO: GSE162028
Experimental models: Organisms/strains		
Sprague-Dawley rat (SPF)	Experimental Animal Center of Nantong University	SCXK(Su)2019-0001
Software and algorithms		
ImageJ	Schneider et al. (2012)	https://imagej.nih.gov/ij
NeuronJ-1.4.3	Meijering et al. (2004)	http://www.imagescience.org/meijering/software/neuronj/
R for statistical computing-4.1.0	R Core Team (2018)	https://www.r-project.org
Seurat-4.1.0	Butler et al. (2018)	https://satijalab.org/seurat/

(Continued on next page)

Continued

REAGENT or RESOURCE	SOURCE	IDENTIFIER
clusterProfiler-4.0.5	Yu et al. (2012)	https://bioconductor.org/packages/release/bioc/html/clusterProfiler.html
DESeq2-1.32.0	Love et al. (2014)	https://bioconductor.org/packages/release/bioc/html/DESeq2.html
WGCNA-1.70	Langfelder and Horvath (2008)	https://horvath.genetics.ucla.edu/html/CoexpressionNetwork/Rpackages/WGCNA/
ARACNe2	Margolin et al. (2006)	http://califano.c2b2.columbia.edu/aracne
ssMARINA-1.01	Aytes et al. (2014)	https://figshare.com/articles/dataset/ssmarina_R_system_package/785718
GSEA-4.1.0	Subramanian et al. (2005)	https://www.gsea-msigdb.org/gsea/index.jsp
FIMO-5.4.1	Grant et al. (2011)	https://meme-suite.org/meme/tools/fimo
pySCENIC-0.11.2	Aibar et al. (2017)	https://github.com/aertslab/pySCENIC
AUCell-1.14.0	Aibar et al. (2017)	https://bioconductor.org/packages/release/bioc/html/AUCell.html
HISAT2-2.0.4	Kim et al. (2015)	http://daehwankimlab.github.io/hisat2/
HTseq-0.6.0	Anders et al. (2015)	https://github.com/htseq/htseq
CIBERSORT	Newman et al. (2015)	https://cibersort.stanford.edu/

RESOURCE AVAILABILITY

Lead contact

Further information and requests for resources and reagents should be directed to and will be fulfilled by the lead contact, Jian Yang (dna2009@ntu.edu.cn).

Materials availability

This study did not generate new unique reagents.

Data and code availability

All sequencing data generated in this study have been deposited in the China National GeneBank Data-Base (CNGBdb) under accession number CNP0002605. Gene expression exploration of this study could be easily accessed at web-based MNniches-seq (<http://121.41.67.1:3838/MNniches-seq/>). Custom scripts and any other relevant data are available from the corresponding authors upon reasonable request.

EXPERIMENTAL MODEL AND SUBJECT DETAILS

Animals

Adult Sprague-Dawley (SD) rats (male, weighted ~200g, provided by the Experimental Animal Center of Nantong University) were housed under standard conditions with a 12-h dark/light cycle and had free access to food and water. The rats were randomly divided into seven groups (naive, injured timepoints: 0.5, 3, 12h, 1, 3days, and 7days) to be deeply anesthetized by an intraperitoneal injection of a compound anesthetic (chloral hydrate 4.25 g, magnesium sulfate 2.12 g, sodium pentobarbital 886 mg, ethanol 14.25 mL, and propylene glycol 33.8 mL in 100 mL) at a dose of 0.2–0.3 mL/100 g.

METHOD DETAILS

Nerve crush

The bilateral sciatic nerve crushed models were conducted as follows: the sciatic nerve was lifted from the right hindlimb on the lateral aspect of the mid-thigh and a 1-cm segment was clamp-injured with a sterile forceps for 30 s. After crush injury, the muscle was then sutured. One group was euthanized immediately and the other groups at hours, 0.5, 3, 12h, and days 1, 3, 7 were euthanized after surgery. All animal experiments in this study were performed in accordance with the guidelines for animal care and were approved by the Administration Committee of Experimental Animals of Jiangsu.

Tissue preparation and rapid staining of MNs before laser capture microscopy

All dissection tools and work surfaces were cleaned with RNase ZAP wipes. Animals were anesthetized by the compound mentioned above and sacrificed by decapitation. The lumbar intumescence part (L4 and L5) of the spinal cord was rapidly removed, immediately embedded in a pre-cooled OCT compound on dry ice to avoid thawing of the tissue. Thin coronal sections (30 μm) were cut at -20°C using a cryostat (Leica CM3050 S) and placed onto PEN Membrane Slide (Leica). Slides were allowed for complete dehydration in the dry box for 10 min at -20°C . Slides containing tissue sections were incubated with Alexa Fluor® 488 Anti-Choline Acetyltransferase antibody (ChAT, 1:50 dilution, Abcam) for 20 min at 4°C , in dark. After being washed with DEPC water, keep the slides into the dry box at 4°C for 20 min until they were dried. All steps were performed on ice and all aqueous reagents were freshly prepared with DEPC water for each experimental day.

Laser capture microscopy

Preheat the Leica LMD6500 Laser Microdissection System and shut on the CTR6500 controller. Placed slides into the slide holder and captured neurons of anterior crus in the spinal cord which were labeled green signal. To avoid damage MNs and ensure a single MN was contained as possible, we cut circular outlines with 1.5–2 times the diameter of obvious MN morphology, and MNs with a visible nucleus in the ventral horn of the spinal cord were dissected. Cells were cut at 40 \times magnification while keeping laser power to a minimum. The Leica system uses gravity to collect cells, which fall into the cap of the collection tube (0.2 mL RNase free PCR tubes) that is placed directly under the slide. These tubes were added 5 μL lysis buffer acquired from Annoroad Gene Technology Co. Ltd. company in advance. Samples were centrifuged in a table centrifuge for 10 s. The tubes were carefully sealed with parafilm (Pechiney Plastic Packaging), labeled, and snap-frozen on dry ice. The whole process from thawing the slides until sample freezing never took longer than 3 h in any of the experiments. Samples were kept in collection tubes at -80°C until further processing.

Smart-seq2 procedure for cDNA library preparation and sequencing

The cDNA sequencing library was prepared as follows the Smart-seq2 protocol (Picelli et al., 2013), including cell lysis, cDNA synthesis, PCR amplification and purification, and quality control. Qualified libraries were then sequenced using the Illumina HiSeq Xten platform. Library construction and sequencing in this study were conducted by Annoroad Gene Technology Co. Ltd. Company.

Immunofluorescence histochemistry

Under anesthesia, the animals were perfused with normal saline and 4% paraformaldehyde. Lumbar intumescence parts of the spinal cords were excised. The samples were post-fixed in 4% paraformaldehyde for 8 h, dewatered in 10%–20%–30% sucrose, and cut on a cryostat into 12 μm thick sections. The immunofluorescent staining was performed using rabbit anti-IBA1 antibody (1:1000 dilution, Abcam), mouse anti-ANXA3 antibody (1:1000 dilution, 11804-1-AP, Proteintech), rabbit anti-ARID5A antibody (1:100 dilution, SAB2100148-100UL, Sigma-Aldrich), mouse anti-ATF3 antibody (1:100 dilution, ab58668, Abcam), rabbit anti-ChAT antibody (1:250 dilution, PA5-29653, Invitrogen), and mouse anti-NeuN antibody (1:250 dilution, MAB377, Sigma) and Hoechst 33342 (1:3000 dilution, Abcam), respectively. The samples were incubated with the primary antibody at 4°C for 12 h, followed by further reaction with the secondary antibody (Goat anti-Mouse IgG-Alex-488, 1:500; Goat anti-Rabbit IgG-Cy3, 1: 100) at room temperature for 1 h. At last, images were taken under fluorescence microscopy (Leica, Germany).

DRG neuron culture and siRNA transfection

DRGs were dissociated from adult male Sprague-Dawley rats (200–220g, Provided by Experimental Animal Center of Nantong University, Nantong, China). DRGs were digested with 0.1% collagenase type I (Sigma, St Louis, MO, USA) in the oxygenated DMEM (Corning, New York, USA). After 120 min incubation at 37°C , DRGs were transferred into 0.25% trypsin (Thermo Fisher Scientific, Waltham, MA, USA) for more 15 min at 37°C . Then, single-cell suspension was centrifuged for 5 min at 1000 r/min with 15% BSA. After chucking the supernatant, the cells were resuspended and plated with Neurobasal-A medium (Thermo Fisher Scientific, Waltham, MA, USA) enriched with L-Glutamine (1%, Thermo Fisher Scientific, Waltham, MA, USA), B27 supplement (2%, Thermo Fisher Scientific, Waltham, MA, USA), and penicillin-streptomycin (1%, Beyotime, Shanghai, China). Experimental plates were pre-coated with poly-L-lysine (Sigma, St Louis, MO, USA). During the plating, DRG neurons were transfected with siRNAs (OBiO, Shanghai, China) using Lipofectamine

RNAiMAX reverse transfection reagent (Thermo Fisher Scientific, Waltham, MA, USA) according to product instructions. After transfection, the culture medium was changed 16 h later. The sequence of siRNA-Arid5a was sense 5'-CCACUGAGAAGCUGAAGAATT-3', antisense 5'-UUCUUCAGCUUCUCAGUGGTT-3'. The sequence of scramble siRNA was sense 5'-UUCUCCGAACGUGUCACGUTT-3', antisense 5'-ACGUGA CACGUUCGGAGAATT-3'. After cultured purified DRG neurons were transfected with siRNA for 16 h, the medium was changed to remove the redundant siRNA. Then, after another 48 h of culture, the DRG neurons were resuspended with 0.05% Trypsin-EDTA (Gibco, Carlsbad, CA, USA) for 1.5 min at 37°C and replanted to experimental plate. 18 h after replant, DRG neurons were fixed with 4% PFA. Neurites were labeled by immunostaining of β -tubulin (Tuj1, 1:500, R&D, Minneapolis, MN, USA), and its immunofluorescence was acquired by Zeiss microscopy (Zeiss, Axio Imager M2m). Total neurite length (only neurite length greater than soma diameter was considered) of each neuron was measured using ImageJ (Schneider et al., 2012) (Neuron J (Meijering et al., 2004), v1.4.3). Approximately 100 cells were analyzed for each condition.

QUANTIFICATION AND DATA ANALYSIS

RNA-seq mapping, quantification, and clustering analysis

Rat genome and annotation were retrieved from the Ensembl database (v89). After trimming low-quality reads, clean reads were mapped against the reference genome with default setting using HISAT2 (Kim et al., 2015). HTseq package (Anders et al., 2015) was used to obtain gene count and normalized into FPKM by considering sequencing depth and gene length. Samples with low expression of *Chat* (FPKM<1) were discarded in the downstream analysis and 682 samples were kept. Sample correlation was estimated based on Pearson's correlation of log₂-transformed FPKM. To estimate neuron signature activity, we used the AUCCell package to calculate the AUC score of neuronal markers. To investigate sample distribution, we performed Principal Component Analysis (PCA) based on log-transformed FPKM using the R program (R Core Team, 2018). UMAP clustering was performed using the Seurat.

Differential expression analysis

DESeq2 package (Love et al., 2014) was employed to detect differential expression genes (DE-Gs). Due to the small DEG number in the early injury stage, we adopt a relatively relaxed threshold that considers both significance and fold-change. Genes with p-value ≤ 0.05 and $|\log_2^{\text{fold-change}}| \geq \log_2^{1.5}$ were defined as DE-Gs compared to the control (naive or corresponding state1). Considering varied sample sizes among different timepoints after sample separation, we further used a bootstrap strategy to detect robust and reliable DE-Gs according to the study (Aguila et al., 2021). Simply as follows.

- Sample sizes were assigned as 3,4,5,6,10, 15/20, ...n, where n is the minimal sample size of the investigated group and the control group. Internal of 5 was used at times points (1, 3ays, and 7days) and internal of 10 was used at timepoints (0.5, 3, 12h).
- For each sample size, we randomly chose samples from two groups respectively. Then performed differential expression analysis with DESeq2 package and screened DE-Gs.
- Repeated b) for 100 times
- The frequency of DE-Gs was calculated.

To define robust DE-Gs, we adopt the threshold, average frequency $\geq 50\%$.

Transcriptional factors (TFs) analysis

SCENIC pipeline (Aibar et al., 2017) was used to perform regulatory network inference and mouse RisTarget motif database (-500-100 bp) was employed. Critical regulons were screened by clustering analysis of connection specificity index (Suo et al., 2018) (CSI) based on area under the recovery curve (AUC) score of regulons (AUC score ≥ 0.1 were considered). ARACNe (Margolin et al., 2006) was also used to reconstruct gene regulatory networks, which was based on an information-theoretic method on large gene expression data. Then, master regulons were inferred by the ssMARINa method (Aytes et al., 2014). ATF3 motif (accession: MA0605) was retrieved from JASPAR database (Fornes et al., 2020) and FIMO (Grant et al., 2011) was used to identify binding sites of *Atf3* in *Arid5a* within 1k bp upstream from the transcription start sites.

Gene set enrichment analysis

Rat geneset were retrieved using the msigdb package. GSEA (Subramanian et al., 2005) was used to perform enrichment analysis. Terms with FDR q-value ≤ 0.25 and NOM p value ≤ 0.05 was defined as a significant enrichment.

WGCNA co-expression analysis

WGCNA package (Langfelder and Horvath, 2008) was applied to construct a single co-expression network and inferred important modules related to axonal injury and regeneration. Firstly, low expressed genes were filtered with row average FPKM < 1 . An automatic, one-step network construction method was employed using the default parameters except for the power of $\beta = 4$. The expression profile of each module was estimated based on the first principal component (module eigengene, ME). The correlation and significance between modules and cell states at each injured timepoints were calculated using the function "cor" and "corPvalueStudent" and adjusted p-value was calculated using the function "p.adjust". The ternary plot-based method could be used for defining expression patterns of triads (Ramirez-Gonzalez et al., 2018). We employed the ternary to explore expression patterns of genes from "turquoise" module along three injured stages (stage1: 0.5, 3, 12h; stage2: 1day from state3; stage3: 3ays and 7days from state2). For each gene from "turquoise", the average expression were normalized against the total expression within the triad to represent the relative expression. The R package "ggtern" was used for the ternary plot (Hamilton and Ferry, 2018). Next, we divided these triads into seven clusters by "20, 20 and 60" rule. For example, if a triad with relative expression in stage1 and stage2 less than 20 while the relative expression in stage3 large than 60, then this triad belongs "Stage3 dominant".

Functional enrichment analysis

ClusterProfiler package (Yu et al., 2012) was used to perform Gene Ontology (GO) and KEGG pathway enrichment analysis.

Public dataset analysis

Time-series course bulk RNA-seq of a long-term investigation of gene expression after rat spinal cord injury (hemi-transection) were retrieved from our previous study (Yu et al., 2019). For the single-cell RNA-seq of spinal cord injury dataset, we retrieved the expression matrix from the GEO database (GSE162610) and performed standard analysis (normalization and standardization) with Seurat (Butler et al., 2018) (V3.0). Original cell type assignment (Milich et al., 2021) was used and expression of key genes was visualized using Seurat. For stranded RNA-seq of wild-type and *Arid5a*^{-/-} mouse MEFs with or without IL6 stimulation were retrieved from the GEO database (GSE178250) and were reanalyzed. DE-Gs identified by comparison expression of Rpl22^{HA} IP in injured and regenerating MNs with the uninjured in mouse spinal cord at 7days post-SNC were retrieved from the supplement (Shadrach et al., 2021). Datasets of single-cell sequencing of DRG sensory (GSE71453) and translome (GSE102316) of *Ils1*-ribotag and *Dhh*-ribotag were retrieved from the GEO database respectively.